

The Stellar Number Density Distribution in the Local Solar Neighborhood is North-South Asymmetric

Brian Yanny¹ and Susan Gardner²

¹*Fermi National Accelerator Laboratory, Batavia, IL 60510*

²*Department of Physics and Astronomy, University of Kentucky, Lexington, KY 40506-0055*

ABSTRACT

We study the number density distribution of a sample of K and M dwarf stars, matched North and South of the Galactic plane within a distance of 2 kpc from the sun, using observations from the Ninth Data Release of the Sloan Digital Sky Survey. We determine distances using the photometric parallax method, and in this context systematic effects exist which could potentially impact the determination of the number density profile with height from the Galactic plane — and ultimately affect a number density North-South asymmetry. They include: (i) the calibration of the various photometric parallax relations, (ii) the ability to separate dwarfs from giants in our sample, (iii) the role of stellar population differences such as age and metallicity, (iv) the ability to determine the offset of the sun from the Galactic plane, and (v) the correction for reddening from dust in the Galactic plane, though our stars are at high Galactic latitudes. We find the various analyzed systematic effects to have a negligible impact on our observed asymmetry, and using a new and larger sample of stars we confirm and refine the earlier discovery of Widrow et al. of a significant Galactic North-South asymmetry in the stellar number density distribution.

Subject headings: Galaxy: kinematics and dynamics — solar neighborhood

1. Introduction

Our own Milky Way Galaxy is a spiral galaxy composed of stars, gas, dust — and a significant amount of dark matter (Gilmore et al. 1989). While matter beyond that provided by disk stars and gas is required to stabilize the Milky Way’s disk (Ostriker & Peebles 1973), the distribution and density of that additional, apparently dark, matter is poorly known (see, e.g., Bovy & Tremaine (2012) and Garbari et al. (2012)). Disk systems are not static,

and while the literature on the azimuthal and radial dynamics of spiral systems is vast, less attention has been given to studies of disk dynamics in the vertical direction.

The finding of Widrow et al. (2012) (hereafter W12) that there appears to be a significant (peak amplitude of $\sim 10\%$) vertical wave in the number of stars within 1 kpc of the sun is surprising and at odds with a history of models of the disk as symmetrical and static in the vertical direction. It suggests that the Galaxy is not in as close to a state of equilibrium in the vertical direction as is frequently assumed, and there may be events in the Galaxy’s recent past driving this and similar vertical waves (Gomez et al. 2013). The unexpected nature of this result makes it worth revisiting with a larger sample of stars over a larger range in Galactic longitude, while paying special attention to possible systematic effects which could affect the number counts above and below the Galactic plane.

The systematics which we explore are largely connected to our use of a photometric parallax relation to determine the distance to a star. In this the intrinsic luminosity of a main-sequence star is inferred from its color, so that its distance follows once its apparent magnitude is measured. Systematic errors also arise from the confusion of dwarfs with giants, from the existence of unresolved binaries, and from stellar population differences, particularly in age and metallicity. The stars we consider are well above the Galactic plane, but we also consider possible inadequacies in the application of corrections for reddening and extinction due to dust. To these ends we explore the dereddened colors of distant halo turnoff stars as a function of Galactic longitude as well. Finally, the location of the sun from the Galactic plane is also a systematic, in that its value impacts the precise shape of the distribution of stars with respect to the Galactic plane, though the inclusion of this effect does not reduce the significance of the asymmetry we observe. Indeed, we find that none of these effects can have a significant effect on the large ($\sim 10\%$) asymmetry we observe in the stellar number counts North versus South.

This paper provides the background error analysis for the results of W12 and precedes the forthcoming paper (Gardner et al., in preparation), which simultaneously analyzes North-South and left-right (Humphreys et al. 2011) asymmetries and discusses their dynamical implications. In anticipation we present here the North-South asymmetry as a function of Galactic longitude as well.

2. Data Selection

We employ photometric and astrometric observations from SDSS DR9, the Ninth Data Release (DR9) of the Sloan Digital Sky Survey (SDSS) (Ahn et al. 2012). DR9 is similar to

the Eighth Data Release (DR8) (Aihara et al. 2011), in that it has the same photometric imaging footprint, including a significant area of approximately 1000 square degrees over which the same Galactic longitude range is covered at moderate Galactic latitudes, avoiding the Galactic plane, of equal and opposite sign. DR9 does correct an earlier issue with the astrometry of DR8, which affected positions and proper motions of a small subset of stars with $\delta > 41^\circ$. In fact, we have used the measured proper motion of M67 to identify its stars, but that cluster is at sufficiently low δ that it is unaffected by this change. The photometry from DR9 is also remeasured separately from earlier SDSS data releases, and this has possible effect on the calibration of photometric parallax relations. We consider this explicitly. One further difference between DR9 and earlier SDSS imaging releases is that the DR9 release does not resolve the centers of dense clusters into individual stars as well as in earlier releases, such as in the Seventh Data Release (DR7) (Abazajian et al. 2009). These issues mean that when we test photometric parallax relations on known clusters, we find differences between different SDSS data releases. These differences, however, are demonstrably small, and in fact have negligible impact on the asymmetry.

The same telescope, instrument, and software reduction system have been used to determine both the North and South data sets, and this gives us confidence that most of the systematic effects which could affect an asymmetry in the star counts have largely “cancelled out.” Nevertheless, issues remain, specifically regarding inadequacies in the reddening corrections, which differ in the North and South, as well as large-scale calibration offset differences, both of which could mimic stellar population differences. We analyze these in more detail than could be done in the limited space of W12.

To minimize obfuscation from dust, we consider high Galactic latitudes, so that the viewing is well out of the Galactic plane. We thus assume that all of the stars we select are beyond the dust, which is thought to lie at $|z| < 125$ pc (Marshall et al. 2006) — this study is for $l < 100^\circ$ only, but Fig. 19 of Berry et al. (2012) reveals that the dust scale height actually increases as one goes to the Galactic center, making the assessment of Marshall et al. (2006) a conservative one for our analysis. Throughout we convert from the observed apparent magnitudes in the SDSS *ugriz* filters to “dereddened” ones, denoted by a “0” subscript, using the extinction maps of Schlegel et al. (1998). The dust maps depend on the Galactic longitude l and latitude b and are rather different in the North and South, though the effects of dust are substantially reduced at the higher latitudes which we employ here. Moreover, for our stars, which are predominately late K and M dwarfs, the vast majority of the region in both the north and south has extinction $E(B - V) < 0.05$. Specifically, using the Schlegel et al. (1998) maps, we note that less than 1% and 5.6% of the area in the North and South, respectively, has $E(B - V) > 0.1$.

We have recently studied (W12) a data set selected as per the following criteria: namely, stars with Galactic coordinates with $100^\circ < l < 160^\circ$ and $54^\circ < |b| < 68^\circ$ that also reside within a perpendicular distance of 1 kpc from the line extending directly up and down from the sun in the vertical coordinate z . Limiting the r_0 -band magnitude such that $14 < r_0 < 21$ and $0.6 < (r - i)_0 < 1.1$ yields a data set of some 300,000 (0.3 M) stars. The study of this data set yields a significant North-South asymmetry which has the appearance of a wavelike perturbation. In this paper we select a similar but non-identical data set, to investigate whether we can confirm the North-South asymmetry observed in our earlier data set. Moreover, if an asymmetry is present and is indeed the result of a perturbation, it is possible that it is localized to particular Galactic longitudes in the neighborhood of the sun. We will pursue this possibility explicitly in Gardner et al. (in preparation), and this predicated the use of a data set with broader coverage in l . We thus select the stars of our present study under slightly broader criteria. The selected stars from SDSS DR9 satisfy the constraints $60^\circ < l < 180^\circ$ and $50.3^\circ < |b| < 59^\circ$, with $13.0 < r_0 < 21.5$ brightness but without saturation yielding a sample of some 3.7 M stars. The selection in (l, b) is shown in Fig. 1. Restricting to $0.6 < (r - i)_0 < 1.1$ as per W12 yields a data set of some 0.85 M stars, comprised of late K and M dwarfs (Covey et al. 2007). We select l, b, r_0 magnitude, $(u - g)_0, (r - i)_0$, and $(g - i)_0$ colors for each star. Note that there is no cut on the distance from the sun imposed explicitly here as there was in W12. For our asymmetry analysis as a function of Galactic longitude, we consider a data set with $0.95 < (g - i)_0 < 2.7$, a sample of some 1.98M stars, comprised of K and M dwarfs (Covey et al. 2007).

The covered region in z and x is shown in Fig. 2; note that this range is also manifestly North-South symmetric and extends to $|z| \sim 2$ kpc. In comparison, the fits of W12 extend to $|z| = 1.6$ kpc. We use r_0 band observations to assess the apparent magnitude of our stars because for the red stars we employ this band offers the greatest signal-to-noise ratio for the range of types of stars, which are K and M dwarfs, in our sample. From these inputs we estimate the distance to each star, albeit with systematic and statistical uncertainties, as we detail in the next section.

3. Photometric Parallax Stellar Distances

The color of a main-sequence star can be used to determine its absolute magnitude through a photometric parallax relation. Although typical random errors for stars at $r = 21.5$ in the SDSS catalog are 7%, after averaging together large numbers of measurements we can reduce the color errors for stars as faint as this magnitude to the level of the systematic error of 1.5% (Padmanabhan et al. 2008) or below. Combining statistical and systematic errors

in quadrature, the associated colors are thus determined to within 3% for even the faintest objects.

We determine the distance to a star in our sample of stars from DR9 using relations constructed using the stars imaged in SDSS DR7, such as those of Jurić et al. (2008), in $(r - i)_0$ color, and of Ivezić et al. (2008), in $(g - i)_0$ color, respectively. To employ the photometric parallax method we have made a number of implicit assumptions, whose assessment ultimately lead to estimates of systematic errors. They concern i) the *identification* of the stars in the survey, i.e., whether they are single, main-sequence stars or not, ii) the neglect of *unmeasured properties* such as stellar metallicity or age on the determined distance, iii) the role of *dust* in the context of our use of the Schlegel et al. (1998) maps, and iv) *large-scale calibration* issues between non-contiguously connected regions of the sky. We will consider each of these possibilities, and in each case we provide detailed, observational tests of our procedures.

To begin with, however, we test and calibrate the photometric parallax relations we employ by applying them to the study of stellar clusters at known distance. Of these, we choose clusters out of the Galactic plane containing stars of comparable color and metallicity to those in our data set. These criteria severely limit the number of clusters we can employ; indeed, the clusters M67 (NGC 2682) and NGC 2420 turn out to be the only suitable candidates. Both clusters have been imaged (once) by the SDSS and were released in both DR7 and DR9. The image processing was similar but distinct in the two cases. The primary difference was that the processing in DR7 ran with a longer timeout, so that it resolved stars appearing deeper towards the centers of these clusters than in DR9 (Aihara et al. 2011). The final photometric calibrations of DR7 and DR9 were performed separately using methods described in Padmanabhan et al. (2008). We calibrate the photometric parallax relations we use with cluster data from DR7. Note that relations used in this paper and in W12 differ in that different procedures to assess cluster membership were employed in the two cases. Here we advocate a more refined procedure, as we shall describe. We also evaluate the impact of the shift from the use of DR7 to DR9 reductions quantitatively.

We employ photometric parallax relations devised by Jurić et al. (2008) in $(r - i)_0$ color and by Ivezić et al. (2008) in $(g - i)_0$ color. The analyses of Jurić et al. (2008) and Ivezić et al. (2008) are based on main sequence fitting to a set of cluster fiducials covering a large range in color. In W12 we used a different zeroth coefficient in each case in order to confront the literature distance to M67 successfully. We have refined that adjustment in our current work. For $(r - i)_0$ color, we begin with the “bright” relation of Jurić et al. (2008), valid over the color range $0.1 < (r - i)_0 < 1.6$, include a correction for the metallicity, and adjust the

constant term in order to confront the cluster distances we have noted. In W12 we employed

$$M_r = \Delta M_r([\text{Fe}/\text{H}]) + 2.38 + 13.30(r - i)_0 - 11.50(r - i)_0^2 + 5.40(r - i)_0^3 - 0.70(r - i)_0^4 \quad (1)$$

for the absolute magnitude M_r , noting a metallicity correction $\Delta M_r([\text{Fe}/\text{H}]) = -1.11[\text{Fe}/\text{H}] - 0.18[\text{Fe}/\text{H}]^2$ (Ivezić et al. 2008), with $[\text{Fe}/\text{H}]$ in dex characterizing the metallicity. We assume a universal $[\text{Fe}/\text{H}] = -0.3$ in our analysis of K and M dwarf field stars; however, as we proceed out of the Galactic plane in $|z|$ we expect the fraction of stars (i.e. a thick disk population) with a metallicity content of $[\text{Fe}/\text{H}] \sim -0.8$ to increase. If $[\text{Fe}/\text{H}] = -0.8$, the assessed distance would be off by some 200 pc, or some 20% on 1 kpc. Our systematic distance error at any given height is a small fraction of this. This systematic error in distance for low-metal, thick-disk stars could potentially impact the location of the second peak in our asymmetry somewhat. We note, then, that the final constant term in color for these stars evaluates to some 0.50 mag less than that employed in Jurić et al. (2008). Although this may seem like a large offset it will not turn out to be so. One reason for this is that the stars used to calibrate Jurić et al. (2008) and Ivezić et al. (2008) were much bluer and essentially disjoint from the red stars used to calibrate our version of their photometric parallax relations. In performing the current analysis, we realized that the large offset we found was driven by our simple assessment of cluster membership in M67 and NGC 2420, which we amend here. In the current paper we employ a constant term of 3.2 in Eq. (1), which is just that of Jurić et al. (2008), though we allow for a metallicity correction of $\Delta M_r([\text{Fe}/\text{H}])$ as well, unlike that work. Note that both the current analysis and that of W12 were adjusted to yield the literature distances to the clusters; the play of some 20% in the distance assessments is a consequence of the manner in which we deduced cluster membership — it is removed once the membership criteria are sharpened. Thus we investigate these issues in careful detail. The $(g - i)_0$ relation of Ivezić et al. (2008), for $0.2 < (g - i)_0 < 4.0$, comes from confronting DR7 SDSS globular cluster data with $(g - i)_0 \lesssim 1$, and the shape of the extension to redder colors was developed from the “bright” relation of Jurić et al. (2008), over the color range $0.1 < (r - i)_0 < 1.6$. For $(g - i)_0$ color, we start with the relation of Ivezić et al. (2008) and adjust the constant term in order to confront the cluster distances we have noted. In W12 we employed

$$M_r = \Delta M_r([\text{Fe}/\text{H}]) - 1.22 + 14.32(g - i)_0 - 12.97(g - i)_0^2 + 6.127(g - i)_0^3 - 1.267(g - i)_0^4 + 0.0967(g - i)_0^5, \quad (2)$$

where we used precisely the same metallicity correction in both color bands. We note that our constant term for these stars is some 0.66 mag less than that employed in Ivezić et al. (2008). This shift, too, is a consequence of our assessment of cluster membership. In the current

paper we employ a constant of -0.50 , which is 0.06 mag greater than the constant in Ivezić et al. (2008). Finally, we estimate the distance d (in parsecs) to a star with intrinsic magnitude M_r and apparent magnitude r_0 via the standard relation $r_0 - M_r = -5 + 5 \log_{10} d$. The analysis of Jurić et al. (2008) has been used to study the stars of the local solar neighborhood, particularly to the end of determining the height of the sun with respect to the Galactic plane. In comparing the stars selected for our asymmetry analysis with those of that study, our sample is not as red in color so that it does not go as close to the Galactic plane. Moreover, our estimated offset of the intrinsic luminosity, as per the reference distance to stars of a more limited color range, also pushes our stars somewhat farther away.

In what follows we reexamine these photometric parallax relations in detail using the observations of main sequence K and M dwarf stars in our two chosen reference clusters, paying careful attention to cluster membership and other systematic effects. We calibrate the photometric parallax relations we use with cluster data from DR7. We then employ our calibrated relations to study the distance to the stars from the same clusters in the DR9 data set, to examine whether any additional adjustments of the photometric parallax relations are necessary. We wish to realize the sharpest assessment of the photometric distance possible, making analysis choices driven by data independent of our asymmetry sample in order to realize an accurate assessment of its shape.

We begin with the cluster M67, for which proper motion information is available (and which we did not exploit in W12). Figure 3 shows the proper motion of stars in and around the field of M67. There are two distinct loci, that of stars in M67 itself and that of a somewhat broader set of stars clearly separated from M67. These are Milky Way field stars. The preliminary membership cut was based on an empirical look at the one-dimensional histograms of μ in each coordinate ($\mu_\alpha \cos \delta$ and μ_δ). The cut was slightly refined by displaying candidate members in a color-magnitude diagram and finding a reasonably small number of outliers. We have made the following proper motion cuts: $-16 < \mu_\alpha \cos \delta < -8$ mas yr $^{-1}$ and $-6 < \mu_\delta < 3$ mas yr $^{-1}$. No objects with a proper motion error greater than 5 mas yr $^{-1}$ in either coordinate are included. A histogram of proper-motion errors shows a modal value of about 2.5 mas yr $^{-1}$. Figure 4 shows a $((g - r)_0, r_0)$ color-magnitude diagram (CMD) of DR7 stars near the position of the cluster M67 which have proper motions consistent with it. A cursory glance at Fig. 3 shows that the Milky Way field in this direction has an average proper motion significantly offset from the M67 average proper motion, so that this procedure removes most field stars, but there is some overlap.

While the proper motion cut significantly decreases outliers, there remain several field stars which stand out in the CMD. Also, there is a clear sequence of unresolved, roughly equal-mass binaries sitting approximately 0.7 mag above the main sequence. These, as

well as the obvious field stars, are separated with simple diagonal cuts and are indicated with open symbols. The filled circles represent our “cleaned” sample used to calibrate our photometric parallax relations. Roughly half of all stars are in binaries, as borne out by explicit study of the M67 cluster (Fan et al. 1996). However, since the luminosity of a main-sequence star scales as its mass raised to the power 3.5, the distance to a sufficiently unequal-mass binary can nevertheless be reasonably evaluated through use of a photometric parallax relation — upon assuming that the heavy companion were alone present. A star which is 2.5 times brighter than another is approximately 1.0 less than it in magnitude; thus we see that evaluating the magnitude of a binary of main-sequence stars by replacing it with the heavier star of them yields magnitude shifts of 0.75, 0.57, 0.41, and 0.28 for a binary with stars in a mass ratio of 1.0, 0.9, 0.8, and 0.7, respectively. The appearance of binaries smears the locus of points in the connection of color to intrinsic luminosity and thus limits the precision to which we can assess the distance — this will be reflected in the scatter of distances we determine to the stars in the cluster, which we will assess as a statistical, or random, error. Studies of the mass-ratio distribution shows that binaries occur more frequently in relatively close mass pairs, both in the M67 cluster, noting Fig. 14 of Fan et al. (1996), and for solar-like stars in the Milky-Way field, noting Fig. 16 of Raghavan et al. (2010). The presence of such like-mass binaries smear the color-luminosity relation the most and thus, from the perspective of distance assessment, are the most problematic; however, from visual inspection of Fig. 4 we see that they are only some 10% of our cluster stars. We identify 27 of such objects in DR7, which we presume are binaries with mass ratios of 0.9 or greater; this number compares closely to the some 30 stars noted in Fig. 14 of Fan et al. (1996). Although equal-mass binaries must also be present in our field stars, possibly with equal probability, we have omitted correcting for a fraction of these objects in our calibration of our photometric parallax relation because we believe it best to sharpen the distance determination of the preponderance of stars in our sample. We note that this cleaning procedure was not effected in the calibration used in W12, so that we can test the impact of this choice through the comparison of our results with those of W12. Let us remark in advance that we observe no changes which would be predicated by this.

Figure 5 shows a $((g - i)_0, d)$ diagram after applying the photometric parallax relation of Eq. (2) and employing $[\text{Fe}/\text{H}] = 0.0$ (An et al. 2008b) for the cluster. We also show the $((r - i)_0, d)$ diagram in Fig. 6, which results from using the distance relation of Eq. (1). As for the reference distance to this cluster, we note the recent compilation of Schlesinger et al. (2012); assuming the results therein are independent, we make an error-weighted average, assuming the errors are independent, to find $d_{\text{M67}} = 0.89 \pm 0.06$ kpc. We use this result in what follows, though we note by comparison the distance obtained from the use of empirically calibrated (theoretical) isochrone models is $d = 0.84 \pm 0.01$ kpc (An et al. 2007a).

Ideally the determined photometric distance to a cluster should be independent of the employed color; the extent to which this is practically so is a test of the photometric parallax relation. In Fig. 7 we probe the $(g - i)_0$ color-distance relationship for M67; we show three panels, the first employing Eq. (2) to yield d (in kpc), which we denote as $d[r_0, M_r((g - i)_0, [\text{Fe}/\text{H}])]$. Fitting a linear polynomial in $(g - i)_0$ color to these results, for $0.5 \leq (g - i)_0 \leq 2.7$, yields a small correction amounting largely to a slope adjustment. Specifically we note the corrected distance d is

$$d = d[r_0, M_r((g - i)_0, [\text{Fe}/\text{H}])] + 0.08982(g - i)_0 - 0.0726, \quad (3)$$

and the impact of the use of this correction is shown in the second panel. Our experience with the $(g - i)_0$ fits indicated that the use of a linear correction was sufficient. The third panel shows the result of applying Eqs. (2) and (3) to the DR9 (rather than the DR7) sample. It is apparent that the small correction gives a significantly better fit, and it is also apparent that the SDSS calibration of the DR9 sample is close enough to the DR7 sample that the same photometric parallax relations (with linear slope correction) may be used for both DR7 and DR9. We now proceed to determine how precisely we can assess the cluster distance.

The upper left panel of Fig. 8 shows the DR7 data for the M67 cluster with only the proper motion cut applied. The upper right panel shows the same field with the unresolved binaries removed, as per the “cleaning” procedure we have described, noting the changed scale on the x-axis. The lower panel is the DR9 version of the upper right panel, i.e., the binaries have been removed via a similar procedure and the same proper motion cut has been applied. Each panel shows both a histogram of the distances to the stars in the cluster as well as the results of a Gaussian fit. The fit parameters are listed in small boxes at the upper right of each panel. We list from the top down: the number of stars, the histogram mean and root-mean-square (RMS), as well as the information for the Gaussian fit, for which $f(x) = p_0 \exp(-(1/2)((x - \langle x \rangle)/\sigma)^2)$. That is, we show the χ^2 per degree of freedom, as well as the fit parameters, namely, a constant (p_0), mean ($\langle x \rangle$), and sigma (σ). The two most relevant parameters to compare are the histogram RMS with the sigma from the Gaussian fit. These parameters should agree in the limit of a large number of points if the data set is indeed normally distributed¹. In particular, when a data set has many outliers, the histogram RMS width may be very different from the Gaussian width. For instance, in the upper left panel, the histogram RMS is 0.81, whereas σ is only 0.11. After cleaning, the histogram RMS becomes 0.15, whereas σ becomes 0.08 — the difference has shrunk from a factor of eight to a factor of two. Looking at the DR9 sample, after a similar cleaning procedure has been applied, the RMS is 0.2, whereas σ is 0.05, yielding a comparison somewhat worse than the

¹<http://root.cern.ch/php883/viewtopic.php?f=3&t=3968>

fit to the DR7 data. We are not concerned by this because the DR9 data set has only 65% as many stars as the DR7 sample. We regard the difference between the histogram RMS and the Gaussian sigma as an estimate of systematic error, reflective of the presence of non-cluster members, whereas sigma itself provides a statistical error estimate. We combine these two types of error in quadrature, using the results of the upper right panel of Fig. 8, to determine $d[\text{M67}] = 0.89 \pm 0.08(\text{stat}) \pm 0.07(\text{sys})$, reproducing the Schlesinger et al. (2012) distance by construction, to find a total cluster distance error of about 0.11 kpc. For the DR9 set, $d[\text{M67}] = 0.93 \pm 0.05(\text{stat}) \pm 0.15(\text{sys})$ kpc for a total error of 0.16 kpc; the two data sets are clearly compatible. The latter result thus also compares favorably with the average literature value we have determined from Schlesinger et al. (2012), namely, $d_{\text{M67}} = 0.89 \pm 0.06$ kpc. This gives us confidence that we can employ our DR7-tuned photometric parallax relations on the DR9 data set. Note, too, we are able to assess the cluster distance to within $\mathcal{O}(10\%)$. Noting once again the upper right panel of Fig. 8, we can translate the statistical error in the distance to the cluster to a typical error in the distance to a star by multiplying 0.066 by the square root of the number of cluster members, to yield an error of about 0.11 kpc. Consequently, we claim that we can assess the distance to a star in M67 to $\mathcal{O}(10\%)$ as well.

We now turn to the analysis of the cluster NGC 2420, for which we employ a metallicity of $[\text{Fe}/\text{H}] = -0.37$ (Anthony-Twarog et al. 2006; Lee et al. 2008), though other determinations have yielded a range of metallicities (Lee et al. 2008). Figure 9 shows a CMD of members of the cluster NGC2420 from DR9, which have further been culled by only keeping objects with SDSS heliocentric radial velocities compatible with the radial velocity of the cluster, $v_r = 75.1 \pm 5.9 \text{ km s}^{-1}$ (Lee et al. 2008), though Lee et al. (2008) note previous radial velocities measurements ranging from $67 - 84 \text{ km s}^{-1}$. We note that the systematic proper motion of NGC 2420 and that of nearby Galactic field stars do not differ significantly, so that we cannot use the method we employed for M67 to isolate cluster members here. Velocities from SDSS stellar spectra typically have errors of 5 km s^{-1} , so that we do not restrict the cluster membership based on the error in the determined radial velocity and demand only that the velocity itself fall within the interval $65 - 85 \text{ km s}^{-1}$. Since our ability to determine cluster membership is less crisp in this case, we do not try to refine our distance assessment further. Rather, we wish only to apply our present procedure to the stars of NGC2420, as an additional test. We show in Fig. 10 the photometric parallax relation for NGC2420 stars with (small filled circles) and without (open circles) the slope correction derived from M67. The slope correction lessens the variations in the computed distance with color slightly. In Fig. 11 we compare the Gaussian fit to the histogram of NGC2420 distances. We apply the same procedure we used previously for M67 to determine the systematic and statistical distance errors, finding $d(\text{NGC2420}) = 2.5 \pm 0.4(\text{stat}) \pm 0.09(\text{sys})$ kpc for a total distance error of 0.41 kpc. An error-weighted average of the distances given in Schlesinger et al. (2012),

assuming the errors are independent, yields $d_{\text{NGC2420}} = 2.57 \pm 0.13$ kpc. The determinations compare favorably, though the width of the Gaussian fit in this case is much broader than it was for the M67 cluster. This could be reflective of the presence of a range of metallicities within the cluster, giving a basis for the range of metallicities found in studies of selected stars (Lee et al. 2008).

We now repeat our $(g - i)_0$ -based analyses with one based on $(r - i)_0$ color and its associated photometric parallax of Eq. (1), after Jurić et al. (2008). By so doing we wish to show that our assessment of systematic errors is independent of the particular choice of photometric parallax relation. This is also crucial for our ultimate application of these refined relations to the stars of our asymmetry analysis, for we wish to demonstrate that the results which emerge there are also independent of the photometric relation chosen. For this to be a sensitive test, the two relations must be similarly well calibrated. Thus we have repeated the analysis depicted in Fig. 7 using the photometric parallax relation in $(r - i)_0$ color. The determined linear correction in color turns out to be slightly larger in this case, yielding a corrected distance d , namely,

$$d = d[r_0, M_r((r - i)_0, [\text{Fe}/\text{H}])] + 0.1415(r - i)_0 + 0.0436. \quad (4)$$

We have also confirmed that the same correction applied to the distances to the stars in the DR9 data set also yields a reasonably flat distance relation with color, rather comparable to that shown in the third panel of Fig. 7 for $(g - i)_0$ color. While there are star-by-star differences between DR7 and DR9, the corrected photometric parallax relation remains flat — no additional adjustments are needed, and we do not make any. We have made Gaussian fits of the distances to M67, mirroring Fig. 8 for $(r - i)_0$ color. For DR7 we obtain $d(\text{M67})_{(r-i)_0} = 0.88 \pm 0.13(\text{stat}) \pm 0.04(\text{sys})$, whereas for DR9 we find $d(\text{M67})_{(r-i)_0} = 0.89 \pm 0.10(\text{stat}) \pm 0.10(\text{sys})$, very comparable to the $(g - i)_0$ results. We have also studied the NGC2420 $(r - i)_0$ distances before and after applying the M67-derived correction to the NGC2420 candidate members after the radial velocity cut has been applied. In this case the distance refinement yields at best a modest improvement. Finally, the DR9 NGC2420 sample, refined by the radial velocity cut we have described, is fit, which yields $d(\text{NGC2420})_{(r-i)_0} = 2.4 \pm 0.5(\text{stat}) \pm 0.2(\text{sys})$. This distance is also compatible with the reference distance to this cluster.

We conclude that our distance estimates, as well as their precision, are not sensitive to the specific photometric parallax relation we choose. We demonstrate that we are able to recover $\mathcal{O}(10\%)$ statistical distance errors for the cluster for which we have the best membership information. Moreover, we are able to assess the systematic errors incurred quantitatively by our assumption of cluster membership and find that they are no larger than our assessed statistical error. We have employed both parallax relations in the analyses

which follow, and find no marked differences, though we focus on the results determined through use of the $(g - i)_0$ color relation in what follows. We used a $(r - i)_0$ relation in W12; a comparison of the detailed calibrations reveal, however, that the correction required to yield a M67 cluster distance independent of color is smaller in the case of the $(g - i)_0$ relation. Moreover, we find that we can study a somewhat larger interval in z in the $(g - i)_0$ case. Thus we favor this choice in what follows.

3.1. Stellar Identification

Although the great preponderance of the stars in our sample are K- and M-type main-sequence stars, it is possible that giants can appear in our sample as well. Moreover, although their distances are reasonably determined by treating them as single, resolved objects, near-equal-mass unresolved binaries can also be present — the distances to the latter, as we have noted, are not well-treated by this approximation. We consider each of these possibilities in turn.

Our selection $13 < r_0 < 21$ is numerically dominated by faint-end-magnitude stars; this ensures that giants can only play a small role in our sample. Exploiting the full multi-band nature of the SDSS data also permits us to make an explicit numerical bound on their appearance. Figure 12, similar to Fig. 10 of Yanny et al. (2009b), reveals the extent to which giants appear. Giants are visible in color-color space as a small diagonal tail running from $((u - g)_0, (g - i)_0) = (3, 1.4)$ to $(4, 2.2)$. Their numbers are completely swamped by dwarf stars; specifically for the r_0 band selection $14.9 < r_0 < 15.4$, we note that there are only some 30 giants in comparison to roughly 70,000 main-sequence stars, for a pollution of only some 0.04%. Only a fraction of the few giants which do appear in Fig. 12 can appear in the sample which we analyze in this paper. Consequently we conclude that giants have no impact on either the number count asymmetries of W12 or on the asymmetries we present here. Fig. 12 also splits the stars into solid circle (blue) ($b > 0$) and open circle (red) ($b < 0$) subsamples. The distributions of these two samples in color-color space, while not identical, lie on top of each other, suggesting there is no gross stellar population difference, i.e., from either metallicity or age, in these two sub-populations. We return to this point in the next section.

We now turn to the possibility of unresolved, equal-mass binaries in our sample. Figure 4 shows a locus of stars shifted about 0.7 mag brighter than the single star locus for the cluster M67; it seems that some 10% of the stars are near equal mass unresolved binaries (Fan et al. 1996). In the general field, we note the study of solar-like stars using data from *Hipparcos* (Raghavan et al. 2010): Fig. 16 of that reference shows that 17 of 110 binaries have

a mass ratio of 0.9 or greater, which is consistent within statistics with our study of M67. Even though we do not correct for this effect in the field, there is nothing different about the way these objects affect apparent star magnitudes above or below the plane, and again, as with the contamination by giants, unresolved binaries cannot not alter the asymmetry results of W12 significantly.

3.2. Role of Unmeasured Properties: Metallicity and Age Effects

How do unmeasured properties such as age and metallicity impact the assessed distances to our stars? Stellar age is a particularly straightforward issue for us, since we are dealing nearly exclusively with stars (K and M dwarfs) which have not yet begun to evolve off the main sequence. A spread in the ages of these stars will not have a significant effect on their colors until they do so. Moreover, the impact of very young stars is also not an issue. The minimum height above the plane for our stars is no less than 300 pc, so that we are also confident that the vast majority of our stars ($> 99\%$) are already on the main sequence and have standard color-magnitude relations for main sequence K and M stars (Jurić et al. 2008). T Tauri stars and other young stars which may still be on their descending Hayashi track to the main sequence are restricted to distances much closer to the plane. In particular, the scale height of molecular gas, where essentially all stars are born is only 74 pc (Dame et al. 1987). The role of metallicity is a more difficult issue. Attempts to determine metallicity from photometry only (Ivezić et al. 2008) almost invariably rely on the determination of u -band-connected colors because such colors are the most sensitive (for SDSS filters) to the presence or absence of the line-blanketing effects of UV atomic metal transitions. While we have access to the u -band magnitudes and $u - g$ colors for our stars, we do not have sufficient precision in the u band to develop a sufficiently accurate photometric proxy for the metallicity. Nevertheless, our Fig. 12, with its closely overlapping North and South dwarf stellar loci, crudely demonstrates the absence of a strong shift in the average metallicity of the two samples. Although vertical and radial gradients in the metallicity are known (Chen et al. 2011), the existence of possible north-south differences have not been documented. Certainly our Fig. 12 offers a simple probe of this issue and suggests that it is unimportant, allowing us to set it aside.

3.3. Testing Dust Corrections

A remaining systematic effect concerns the possibility of inadequately estimated reddening differences between the North and South. While the Schlegel et al. (1998) dust maps

have been shown, using photometry and CMD histograms, to be very accurate (Schlafly et al. 2010), especially for higher latitude ($|b| > 30^\circ$) sight-lines, there remains their finding, which is affirmed with a separate analysis using stars with SEGUE spectra (Schlafly and Finkbeiner 2011), that the stars in the South, working in $(g - r)_0$ color and using a very large scale average, appear to be about 0.02 mag redder than the stars in the North. This result is based on the average colors of blue turn-off stars. The difference in $(r - i)_0$ color is smaller by a factor of three.

There are three possible explanations for the observed color difference. First, there may be a global calibration error in the photometry within the SDSS DR7 (and DR8) releases, which the study of Schlafly et al. (2010) supports, though this, noting Table 4 of Schlafly et al. (2010), does not seem to capture the complete effect. However, the differences in area in the two studies implies that the conclusions of Schlafly and Finkbeiner (2011) need not hold for the photometric study (Schlafly et al. 2010). An offset in the g_0 -band magnitude scale is the most likely because the blue-tip stars in $(r - i)_0$ color are relatively unaffected. Maintaining absolute calibrations to better than 1% across very large areas, especially those which are only nominally contiguous, as it is here with different regions connected only by narrow strips running through the Galactic plane, is an extremely difficult task, subject to many subtle problems. A recent analysis by Betoule et al. (2013) re-examines the large scale calibration of the SDSS with an effort toward improving Type I supernovae (standard candle) distances and finds that there are indeed systematic drifts in the SDSS calibration of some filters at the level of 1% to 2% over 100° scales. Thus we regard it as very possible that such a large-scale calibration drift exists in the g_0 band between the North and South. A second way to explain a global color difference would be a reddening map anomaly. All our colors and magnitudes are corrected for reddening based on Schlegel et al. (1998). We regard a problem with the reddening maps to be unlikely, as we discuss below, but we cannot completely rule out this possibility. A third way to have a global color difference would be through an actual stellar population difference, namely, that the distribution of stellar metallicity is different above and below the Galactic plane. This, too, we think is unlikely, and we discuss it further later.

In order to select among the possibilities, we divide the “blue-tip” stars (turn-off stars of spectral type F extending to the halo of the Milky Way), in our survey region into six 20° segments in Galactic l . We plot the $(g - r)_0$ color histograms of these blue-tip stars in three magnitude bins, namely $18 < g_0 < 19$, $19 < g_0 < 20$, and $20 < g_0 < 21$, and measure the central color and peak heights of each histogram in the north and south samples separately. Since Schlafly et al. (2010) uses $((g - r)_0, g_0)$ CMDs for their analysis of blue-tip stars, we adopt the same analysis for consistency. The results of this analysis are reported in Table 1, and the number count studies and color offsets are also summarized in Fig. 13. Table

1 presents peak $(g - r)_0$ turnoff color for star subsets, namely for $50.3^\circ < |b| < 59^\circ$ and the indicated l range with g_0 restricted to the range given in brackets. The numbers in parentheses indicate the total star counts in the central bin. Note that the number counts of blue-tip stars in each bin should roughly match in the north and south (within Poisson errors), provided the halo is fairly smooth. Within Poisson statistics, only two bins (in boldface) are markedly discrepant — and we will find that they correspond to the angular location and distance of the turnoff stars in the Sagittarius stream.

Generally Fig. 13 and Table 1 show that the number of turn-off stars tends to fall more or less smoothly for a fixed band of g_0 as l increases, i.e., as one looks away from the Galactic center. There is one pair of bins in the South, however, with $20 < g_0 < 21$ and $140^\circ < l < 180^\circ$, which is strikingly inconsistent with that trend. In this case the difference in the number counts in matching bins North and South are several times the square root of the counts in the corresponding bins — suggesting the presence of a structure. In fact these bins in the South are contaminated by Sagittarius stream stars, as can be seen by an examination of Fig. 9 of Yanny et al. (2009a), which clearly shows the Sagittarius stream passing through this l range. The implied distances to the blue-tip stars, that is, $15 < d < 25$ kpc, closely matches that of the distance to the Sagittarius stream stars. Aside from this particular structure present in the South, the relative numbers of blue-tip stars in the North and South are fairly closely matched. We also note that the average colors of the South blue tip stars are systematically a couple of percent redder than the corresponding bins in the North, and these differences persist across four of the 20° longitude bins and three different magnitude bins, the latter corresponding to three different distance bins ranging from some 5 to 25 kpc from the sun. This persistent color difference, which is just what Schlafly et al. (2010) found, argues strongly against the existence of a localized stellar population difference, or a localized “rogue dust cloud,” in either just the North or the South, but rather suggests a global calibration difference. In support of this we show in Fig. 14 the comparison of $(g - i)_0$ and $(r - i)_0$ for stars in our sample. The tight central locus of Fig. 14 which appears without sharp bends, shows that one color may be substituted for the other without large shifts of estimated (photometric parallax) distances. This in itself argues against the possibilities of rogue population or reddening differences. Note that even with this global calibration difference, the star counts made in the North in comparison to those made in the South are not really affected because we see the same asymmetries whether we use the $(r - i)_0$ or the $(g - i)_0$ photometric parallax relation. We have shown, too, by exploring photometric parallax relations in two correlated color ranges, $(g - i)_0$ and $(r - i)_0$, that our distance estimates are independent of the filter used.

4. The North-South Asymmetry

We now proceed to analyze our larger sample in the spirit of W12, to determine the vertical distribution of the stars and finally the North-South asymmetry they possess with respect to the center of the Galactic plane. To do this, we must first determine the appropriate saturation and color cuts. We then construct a selection function in order to estimate the stellar number density as a function of vertical displacement from the sun, given that our stellar sample is restricted to a limited window in b and l . We note that with suitable color cuts the selection function is determined by purely geometric factors. Finally, we fit our inferred “true” vertical distribution of stars to a theoretical form in order to determine the location of the sun with respect to the Galactic plane. With this in hand we can finally determine the North-South asymmetry about the Galactic plane — and we have sufficient statistics to analyze its variation with Galactic longitude as well.

The SDSS data are affected by a selection on the bright end — most objects are saturated if $r_0 < 14.5$. In order to make our saturation limit more uniform in color, we apply a slightly fainter saturation cut (though we used $r_0 = 14$ in W12). Its intended effect is to remove any systematics due to saturation in our asymmetry analysis. Fig. 15 shows that we may remove stars with $r_0 < 15$ — this improves the completeness of the sample on the near end, without significantly losing statistical significance. Fig. 16 shows how the particular $(g - i)_0$ colors of the stars relate to their vertical distances, where we impose $r_0 > 15$ and compute distances as per Eq. (3). The shape of the region is determined by our window on r_0 ; a judicious choice of color interval opens a vertical window on $|z|$ which is not limited by our finite range of r_0 . We note, e.g., that if we choose $1.8 < (g - i)_0 < 2.4$, our sample is complete on the interval $0.3 \text{ kpc} < |z| < 2.0 \text{ kpc}$. In DR9, there are some 794,500 stars which satisfy all our cuts. The selection function is determined by geometry. Since we bin the photometric data with vertical height, the selection function is the effective volume, bin by bin, associated with the observed stars. That is, if the center of a vertical bin is at z , then the selection function $\mathcal{V}(z)$ for our North-South symmetric data sample is

$$\mathcal{V}(z) = \frac{1}{2} \delta (l_2 - l_1) z^2 \left(\frac{1}{\sin^2 b_1} - \frac{1}{\sin^2 b_2} \right), \quad (5)$$

where δ is the bin width in kpc, noting $l \in [l_1, l_2]$ and $|b| \in [b_1, b_2]$ are in radians. Finally we fit the function determined by $n(z) \equiv n_{\text{raw}}(z)/\mathcal{V}(z)$, where $n_{\text{raw}}(z)$ is the number of stars we observe in a vertical bin centered on z . We adopt the same standard Galaxy thin and thick disk model form used in W12,

$$n(z) = n_0 \left(\text{sech}^2 \left(\frac{(z + z_\odot)}{2H_1} \right) + f \text{sech}^2 \left(\frac{(z + z_\odot)}{2H_2} \right) \right), \quad (6)$$

and show the result in Fig. 17, which displays the stellar number density as a function of distance. Already here we see that the deviations of the counts from the best-fit model change sign under $z \leftrightarrow -z$; i.e., they are odd under parity. This is further highlighted in Fig. 18. We have 600 bins over the region $|z| < 2.5$ kpc, so that $\delta \approx 0.0083$ kpc. The fit is over the region with $|z| < 2$ kpc, yielding $\chi^2/\text{ndf} \approx 3.8$, $n_0 = (4.74 \pm 0.04) \times 10^6 \text{ kpc}^{-3}$, $H_1 = 0.232 \pm 0.001$ kpc, $H_2 = 0.666 \pm 0.006$ kpc, $z_\odot = 14.3 \pm 0.6$ pc, and $f = 0.109 \pm 0.002$. Figures 17 and 18 update Fig. 1 in W12. The quality of our fit is markedly better than in W12, due to an improved calibration and saturation-cut choices, though we still reject a North-South symmetric model for $n(z)$. The results of Figs. 17 and 18 evince a North-South asymmetry, strongly confirming the results of W12.

We construct a North-South asymmetry by comparing star counts North and South directly. If we compare, e.g., the raw counts as a function of the vertical displacement from the sun’s location, we define

$$\mathcal{A}_{\text{raw}}(|z|) \equiv \frac{n_{\text{raw}}(|z|) - n_{\text{raw}}(-|z|)}{n_{\text{raw}}(|z|) + n_{\text{raw}}(-|z|)}. \quad (7)$$

This quantity is shown in Fig. 19. Ultimately, however, we would like to determine the North-South asymmetry in terms of the effective stellar number density as a function of the vertical displacement from the Galactic plane. We realize this in two steps. First, we plot the raw asymmetry in terms of $|z + z_\odot|$ as shown in Fig. 19. We then include the selection function as well, in order to compute the asymmetry in terms of the effective number density, namely,

$$\mathcal{A}(|z + z_\odot|) \equiv \frac{n(|z + z_\odot|) - n(-|z + z_\odot|)}{n(|z + z_\odot|) + n(-|z + z_\odot|)}. \quad (8)$$

We use $z_\odot = 14.3$ kpc as per our earlier fit. The North-South asymmetry is visible in the original star number counts, and the refinements we have included in Eq. (8) impact its precise shape but not its significance. At this point it is appropriate to revisit the various systematic effects we have studied earlier in the paper and explore their impact on the asymmetry. Specifically, we consider the role of z_\odot , the impact of our tune of the photometric parallax relation from the fit to M67 data, Eq. 3, and finally the impact of a possible 2% calibration error in the g_0 band, either North or South. The asymmetries which result from these changes are illustrated in Fig. 20. In all cases the resulting asymmetry is still significantly non-zero. However, the impact of the change in z_\odot and in the tilt and offset of the photometric parallax relation away from the optimal values determined in our fits yield significant changes in the shape of our asymmetry. The impact of the possible 2% calibration errors is, in contrast, much smaller.

In Fig. 21 we compare the asymmetry $\mathcal{A}(|z + z_\odot|)$ computed using different color bins; the window on the vertical coordinate for each color band is limited by the saturation and

faintness limits on r_0 in each case, noting, e.g., Fig. 16 for $(g - i)_0$ color. We show the asymmetries for three different bins on $(g - i)_0$ color, namely, $1.40 < (g - i)_0 < 1.8$, $1.8 < (g - i)_0 < 2.4$, and $2.4 < (g - i)_0 < 2.7$. The different asymmetries are reasonably similar where they all coexist. We also compare these results with an asymmetry determined from distances computed using $(r - i)_0$ color, namely Eq. (4). Choosing a sample with $0.6 < (r - i)_0 < 1.1$, we note as per Fig. 14 that this crudely corresponds to $1.8 < (g - i)_0 < 2.4$. Perhaps not unexpectedly, the asymmetry results in these two particular bands compare favorably, though the stars selected by the $(r - i)_0$ cut are a distinct sample — some 852,000 stars satisfy the cuts for this analysis. This particular result confirms, moreover, the findings of W12 with a sample size roughly three times bigger. Interestingly, the close comparison of the results based on the different photometric parallax relations suggests that any possible problem with the large-scale calibration of the g_0 band does not impact the asymmetry significantly; this is supported by our study of Fig. 20 as well.

We consider now the persistently large asymmetry seen in Fig. 21 at larger distances from the plane, $1.4 < |z| < 2.0$ kpc for the bluest color bin, $0.95 < (g - i)_0 < 1.8$. The blue end of this bin corresponds to K-type stars with $(g - r)_0 \sim 0.72$. Could this excess be due to a contamination in this field? We note that giants in the Sagittarius stream’s southern tail are located in our observing window some 15-30 kpc below the plane. Figure 11 from Majewski et al. (2003) shows that only approximately 100 such M giants exist below the Galactic plane. Still, perhaps stars associated with the more populous red giant branch and even sub-giant branch stars associated with Sagittarius could add to the effect. By inspection of our sample, we note that the magnitude and color of the largest excess of stars with $-2 < z < -1.5$ kpc have an average $\langle r_0, (g - r)_0 \rangle = 17.5, 0.63$. These values correspond to a spectral class G/K sub-giant with absolute $M_r \sim 1.6$ (see Fig.3 of Yanny et al. (2009a) for a view of the turnoff of the Sagittarius stream in the North at 45 kpc from the sun, somewhat fainter than the magnitudes explored here), at a distance of about 15 kpc, close to the 15-30 kpc distance range for known Sagittarius stream south stars. Are there enough of them? For every M-giant (noting the ~ 100 seen in Majewski et al. (2003)), there can be 50 sub-giants in an evolving cluster luminosity function of this age and metallicity, though not all of these will have colors as red as $(g - i)_0 > 0.95$. Indeed most subgiant stars are bluer than our bluest cut in Fig. 21. Still a significant portion of these stars are likely to remain. To explore the issue further, we study the asymmetry as a function of the bluest $(g - i)_0$ colors we choose to include in Fig. 22. We see explicitly that restricting the color from $0.95 < (g - i)_0 < 1.8$ to $1.4 < (g - i)_0 < 1.8$ does reduce the number of stars in the South at $|z| \sim 1.5$ kpc. Nevertheless, this change has no impact and significance of the asymmetry we claim at smaller $|z|$, and some asymmetry in the region of $|z| \sim 1.5$ kpc would seem to persist. We have studied the asymmetry split into latitude bins as well, and it

further supports this interpretation, with the finding of a similar asymmetry only in the bin containing Sagittarius stream stars (see Table 1) at $140 < l < 180$ compared with the lower latitude bin ($l < 140$), which shows a smaller asymmetry. While the apparent third peak of the asymmetry remains visible in Fig. 21 at the 3-4% level when we exclude sub-giant contaminants by restricting our choice to redder stars $(g - i)_0 > 1.8$, (corresponding to a late K, early M spectral type) we could have some contamination from Sagittarius giants affecting the amplitude of the third peak at the 1% level. Conversely, there is no evidence that the two larger peaks at $|z| \sim 0.4, 0.8$ kpc could be due to sub-giant contamination from a more distant stream. The asymmetries are color-independent and significantly larger in amplitude than any known stream could accommodate — Sagittarius is the largest known Milky Way halo stream.

Finally we consider the Galactic longitude dependence of the asymmetry. Here we work in $(g - i)_0$ color, choosing the band $0.95 < (g - i)_0 < 2.7$. The analysis sample is shown in Fig. 23; it appears rather uniform, North and South. The number counts differences, North and South, are also shown in Fig. 24; here we see in the raw data a persistent excess of counts in the South, and then in the North, as we move out of the Galactic plane, for a sweep of l . Finally, we report the determined North-South asymmetry in Fig. 25. In the latter we restrict our consideration to the vertical window [0.5 kpc, 1.1 kpc], the range for which the sample is complete. For this larger color swatch there are some 1.98 million stars in our sample. To study the l dependence, we split this sample into three forty-degree-wide l bins. For $60^\circ < l < 100^\circ$, there are some 783,000 stars with a mean $(g - i)_0$ color of $\langle (g - i)_0 \rangle = 1.95$. For $100^\circ < l < 140^\circ$, there are some 635,000 stars with $\langle (g - i)_0 \rangle = 1.97$. For $140^\circ < l < 180^\circ$, there are some 566,000 stars with $\langle (g - i)_0 \rangle = 1.99$. The asymmetry for all l in this color band is shown by the asterisk points in Fig. 25. We note that indeed there appears to be a significant difference in the asymmetry with l , with a smaller amplitude towards the Galactic center. This is naively what one would expect for a disk which gets thicker the closer one gets to the Galactic center; it would be less responsive to a disturbing force. Our forward- and backward-looking samples, noting Fig. 2, probe regions of the disk separated by roughly 1 kpc. The longitudinal angle dependence could also be suggestive of the location of a perturbing influence. In a followup paper (Gardner et al., in preparation), we plan to examine how well-localized the asymmetry may be. We know that there are also effects due to a bar toward the Galactic center which are not completely symmetric north and south, left and right (Benjamin et al. 2005), though such effects do not figure in our present study.

5. Summary and Outlook

In the context of a larger data set we confirm and refine the earlier observation of a large North-South asymmetry in the star counts with respect to the Galactic plane (W12). We observe a peak asymmetry of some 10%, that is, roughly a peak-to-trough difference of 20%.

The strong Jeans theorem states that the matter probability distribution function in steady state can be written in terms of three isolating integrals. One of these becomes the vertical energy E_z , which in turn goes as z^2 , having manifest even parity, as one approaches the Galactic plane (Binney & Tremaine 2008). The appearance of our odd-parity asymmetry can be regarded as either falsifying the expected relationship $E_z \propto z^2$ as one approaches the Galactic plane, or, alternatively, as challenging the notion that the matter distribution function can be written in terms of isolating integrals at all. The “ringing” nature of the asymmetry result we have found strongly favors the latter interpretation. We thus believe the asymmetry speaks to observational evidence for the failure of local gravitational equilibrium, or steady-state dynamics, in the local solar neighborhood.

We regard this as a cautionary tale for analyses which would employ equilibrium assumptions to analyze the local distribution of dark matter. While 20% density differences are well within the uncertainties of the unknown local dark matter distribution, the large velocity tail of the local dark matter phase space distribution is likely much more sensitive to such effects. We note that recent results from the RAVE velocity survey show evidence for vertical ringing in the z -velocity of stars at the same distances discussed here (Williams et al. 2013).

We have considered a wide range of possible systematic effects which could affect the symmetry in the distribution of stars north and south of the Galactic plane. We are able to quantify these systematics to a great extent and rule out giant/dwarf confusion, photometric parallax distance relation differences, reddening corrections, and large scale calibration errors as possible sources of the observed asymmetry. We are able to demonstrate that photometric parallax method based on SDSS photometry gives systematic and statistical distance errors of typically 10% at least for lower main sequence (K/M dwarf) populations. To a more limited degree, we constrain the extent to which the asymmetry can be resolved by equal-mass binary confusion, or metallicity differences, though we cannot rule out these effects completely.

Certain systematic effects are best explored through the study of distant “blue-tip” stars in our sample. By dividing the data into six bins in l and exploring the properties of these stars therein, we are able to state that there are no significant localized reddening

correlations beyond those of the Schlegel et al. (1998) maps. We confirm the slight color difference in $(g - r)_0$ noted by Schlafly et al. (2010), and we find evidence that the most likely explanation for it is a some 0.02 mag difference in the global calibration of the g filter in the SDSS, as it connects the South survey region to the North survey region. We study the asymmetries in both $(g - i)_0$ and $(r - i)_0$ colors and show explicitly that the asymmetry results agree nicely without regard to which color baseline is used.

The $(g - r)_0, (r - i)_0$ colors of our samples are consistent with no significant color differences in the North versus the South. Regarding a possible difference in metallicity gradients, North and South, we do not have sufficient u -band accuracy to perform a photometric metallicity analysis in the manner of Ivezić et al. (2008). Slight systematic differences in the average metallicity of the north versus south populations remain possible. However, no possible metallicity shift would lead to stellar density ringings confirmed here. We note that the persistence of the asymmetries observed in W12 in the current work, determined using a much larger sample of stars in a slightly different portion of the sky, also argues against the existence of idiosyncratic north-south population differences as a source of the effect.

In Gardner et al. (in preparation) we plan to analyze the symmetries associated with multiple integrals of motion simultaneously, in hope of isolating the origin of the asymmetry.

We acknowledge use of SDSS-III data (<http://www.sdss3.org>). We acknowledge contributions from Kathryn Mummah on the study of blue tip stars vs. l , and we thank James Bullock for helpful comments. We acknowledge the anonymous referee for several useful comments which improved the paper. SG acknowledges partial support from the U.S. Department of Energy under contract DE-FG02-96ER40989 and thanks Wolfgang Korsch for expert advice in the use of the ROOT analysis framework. SG thanks Nora Brambilla and the Excellence Cluster “Universe” of the Technical University of Munich for hospitality during the completion of this work.

REFERENCES

- Abazajian, K., Adelman-McCarthy, J.K., Agueros, M.A., et al. 2009 ApJS, 182, 543
- Aihara, H., Allende Prieto, C., An, D. et al. 2011 ApJS, 193, 29
- Ahn, C. P., Alexandroff, R., Allende Prieto, C. et al. 2012 ApJS, 203, 21

- An, D., Terndrup, D. M., Pinsonneault, M. H., Paulson, D. B., Hanson, R. B., & Stauffer, J. R. 2007 ApJ, 655, 233
- An, D., Johnson, J. A., Clem, J. L. et al., 2008 ApJS, 179, 326
- Anthony-Twarog, B. J., Tanner, D., Cracraft, M., & Twarog, B. A. 2006, AJ, 131, 461
- Benjamin, R. A., Churchwell, E., Bable, B.L. et al. 2005 ApJ 630, L149
- Berry, M. Ivezić, Z., Sesar, B. et al., 2012, ApJ, 757, 35
- Betoule, M., Mairiner, J., Regnault, N. et al. 2013 A&A 552, 124
- Binney, J., & Tremaine, S. 2008, Galactic Dynamics: Second Edition (Princeton University Press)
- Bovy, J., & Tremaine, S. 2012 ApJ 756, 89
- Chen, Y. Q., Zhao, G., Carrell, K., Zhao, J. K., 2011, AJ, 142, 8
- Covey, K. R., Ivezić, Z., Schlegel, D. et al., 2007, AJ, 134, 2398
- Dame, T. M., Ungerechts, H., Cohen, R. S. et al. 1987, ApJ, 322, 706
- Fan, X., Burstein, D., Chen, J. S. et al. 1996 AJ, 112, 628
- Garbari, S., Liu, C., Read, J.I., & Lake, G. 2012 MNRAS 425, 1445
- Gilmore, G., Wyse, R. F. G., & Kuijken, K 1989 ARA&A, 27, 555
- Gomez, F.A., Minchev, I., O’Shea, B. W., Beers, T. C., Bullock, J. S., & Purcell, C. W. 2013 MNRAS 429, 159
- Humphreys, R. M., Beers, T.C., Cabanela, J.E., Grammer, S., Davidson, K., Lee, Y.S. & Larsen, J.A. 2011 AJ, 141, 131
- Ivezić, Ž., Sesar, B., Juric, M. et al., 2008a, ApJ, 684, 287
- Jurić, M., Ivezić, Z., Brooks, A. et al. 2008 ApJ, 673, 864
- Lee, Y. S., Beers, T. C., Sivarani, T. et al. 2008, AJ, 136, 2050
- Majewski, S. R., Skrutskie, M. F., Weinberg, M. D., Ostheimer, J. C. 2003 ApJ 599, 1082
- Marshall, D. J., Robin, A. C., Reylé, C., Schultheis, M., & Picaud, S. 2006, A&A, 453, 635

- Ostriker, J. P. and Peebles, P. J. E. 1973, ApJ 186, 467
- Padmanabhan, N., Schlegel, D. J., Finkbeiner, D. P. et al. 2008 ApJ 674, 1217
- Raghavan, D., McAlister, H. A., Henry, T. J., Latham, D. W., Marcy, G. W., Mason, B. D., Gies, D. R., White, R. J., & ten Brummelaar, T. A. 2010, ApJS, 190, 1
- Schlafly, Finkbeiner, Schlegel, Jurić, Ivezić, Gibson, Knapp, & Weaver 2010, ApJ, 725, 1175
- Schlafly, E. F., and Finkbeiner, D. P. 2011 ApJ 737, 103
- Schlesinger, K. J., Johnson, J. A., Rockosi, C. M. et al. 2012 ApJ 761, 160
- Schlegel, D. J., Finkbeiner, D. P., & Davis, M. 1998, ApJ, 500, 525
- Widrow, L. M., Gardner, S., Yanny, B., Dodelson, S., and Chen, H.Y., 2012, ApJ, 750, L41 (W12)
- Williams, M.E.K., Steinmetz, M., Binney, J. et al. 2013 arXiv:1302.2468
- Yanny, B., Newberg, H. J., Johnson, J. A. et al. 2009a ApJ700, 1282
- Yanny, B., Rockosi, C., Newberg, H. J. et al., 2009b, AJ, 137, 4377

Table 1.

l range (in $^\circ$)	$(g-r)_0$ N [20, 21]	S (peak) [20, 21]	N [19, 20]	S [19, 20]	N [18, 19]	S [18, 19]
$60 < l < 80$	0.305 (884)	0.316 (855)	0.300 (673)	0.317 (565)	0.291(484)	0.306(423)
$80 < l < 100$	0.304 (733)	0.320 (651)	0.301 (552)	0.315 (482)	0.287(400)	0.312(342)
$100 < l < 120$	0.304 (591)	0.333 (512)	0.300 (465)	0.324 (373)	0.283(346)	0.309(306)
$120 < l < 140$	0.305 (503)	0.320 (481)	0.302 (400)	0.325 (333)	0.282(317)	0.304(260)
$140 < l < 160$	0.306 (461)	0.299 (690)	0.300 (367)	0.312 (317)	0.283(269)	0.292(243)
$160 < l < 180$	0.304 (484)	0.299 (784)	0.296 (382)	0.306 (302)	0.294(278)	0.294(255)

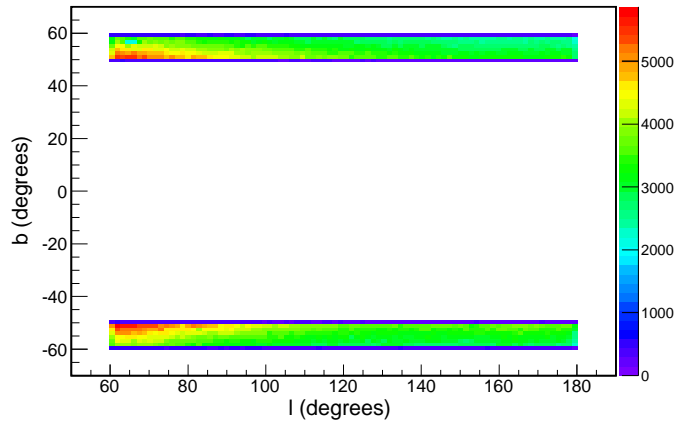


Fig. 1.— A map of b versus l with $13.0 < r_0 < 21.5$ for the stars from SDSS DR9 used in this study. The shading of each bin gives the relative stellar density as indicated by the scale bar to the right of the plot.

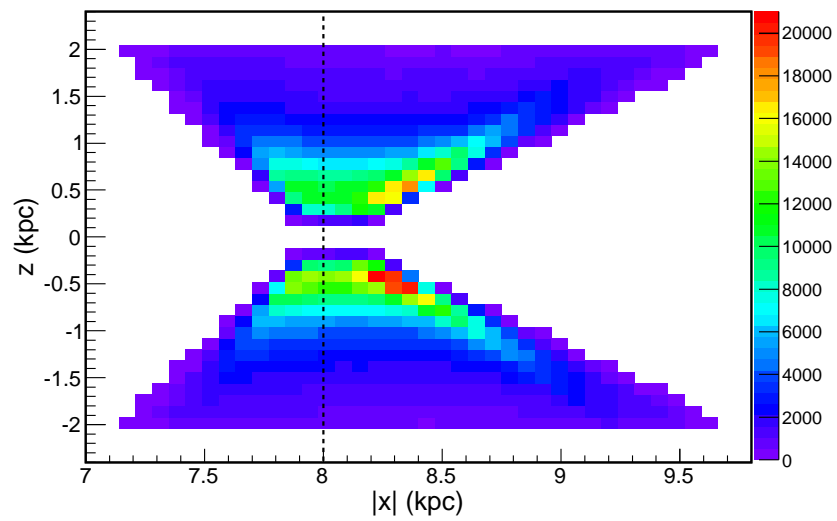


Fig. 2.— Plot of z versus $|x|$ for the stars from Fig. 1 in a coordinate system where the Sun is assumed to be located at $|x| = 8$ kpc. Our data set samples stars both inside and outside the solar circle.

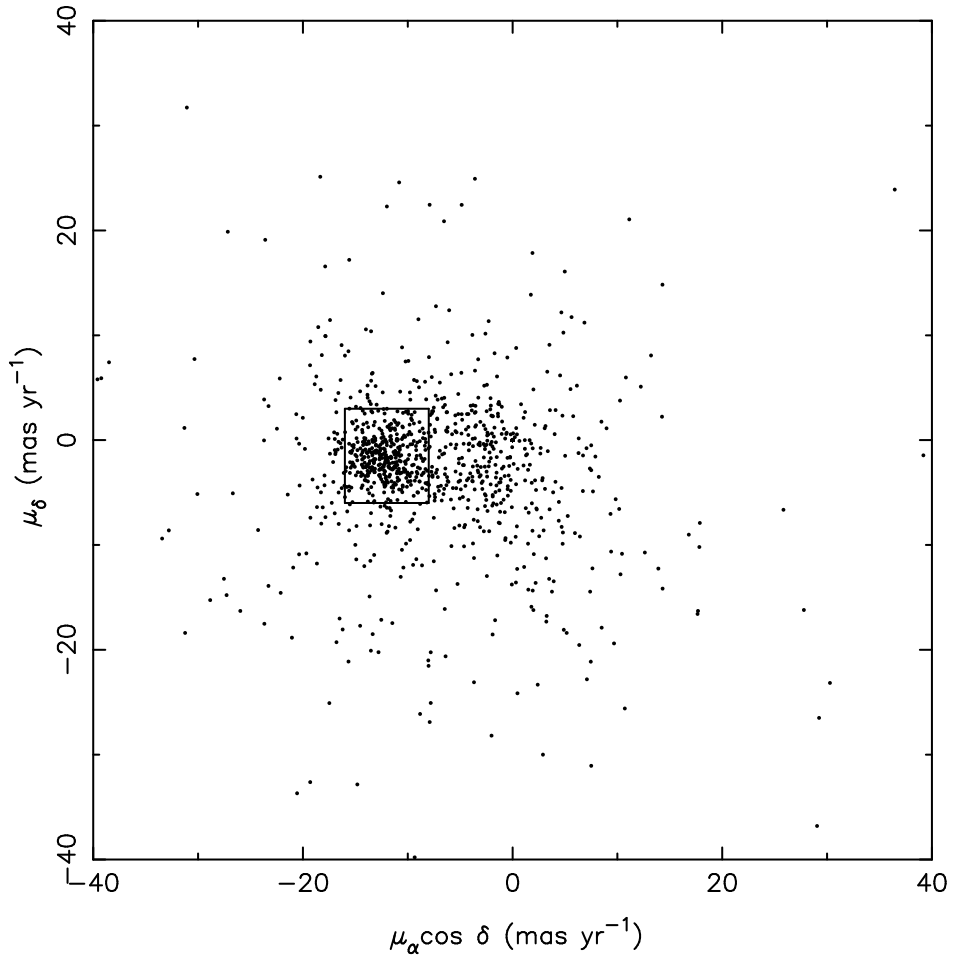


Fig. 3.— Proper motion of stars in the M67 field. The box indicates our M67 membership cuts: $-16 < \mu_\alpha \cos \delta < -8$ mas yr⁻¹ and $-6 < \mu_\delta < 3$ mas yr⁻¹. Only objects with proper motion errors $\sigma(\mu_\alpha \cos \delta, \mu_\delta) < 5$ mas yr⁻¹ are included in the the M67 sample.

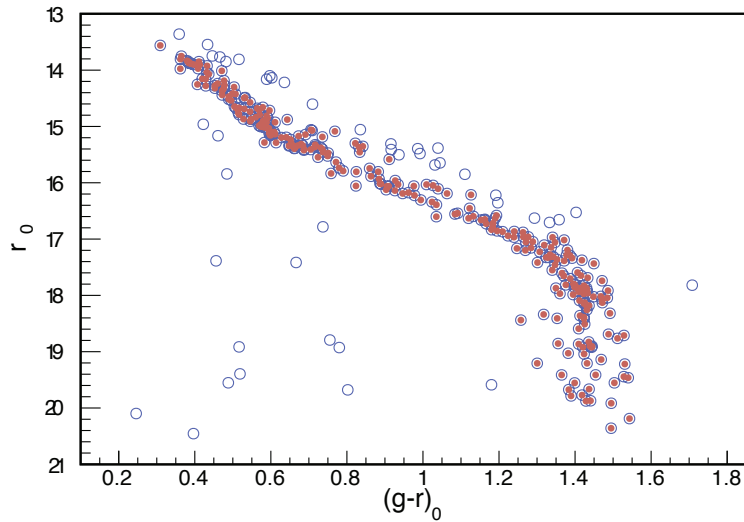


Fig. 4.— A color magnitude diagram of SDSS DR7 stars presumed to be in M67 from the proper motion selection box in Fig. 3. Filled circles represent objects which lie along the stellar locus and which are neither equal-mass binaries nor obvious field stars — they represent our cleaned M67 membership sample.

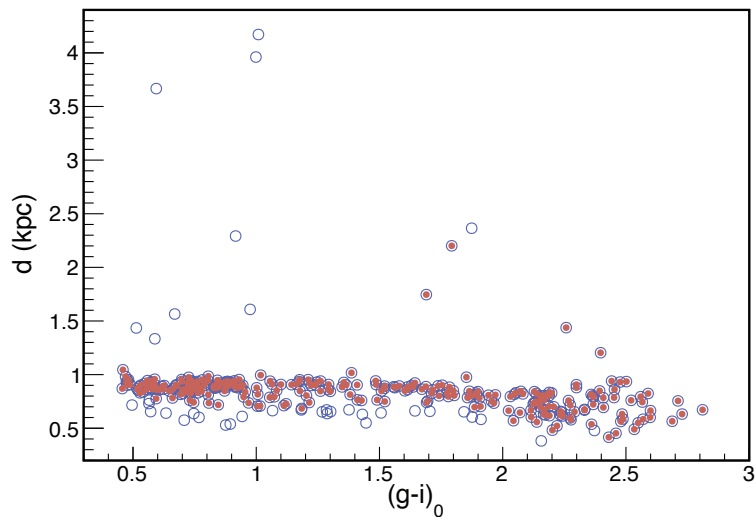


Fig. 5.— The proper motion selected (all circles) and cleaned (filled circles) DR7 samples from Fig. 4, now plotted with photometric parallax distance versus $(g - i)_0$ color. There is a slight trend with color for these equidistant points.

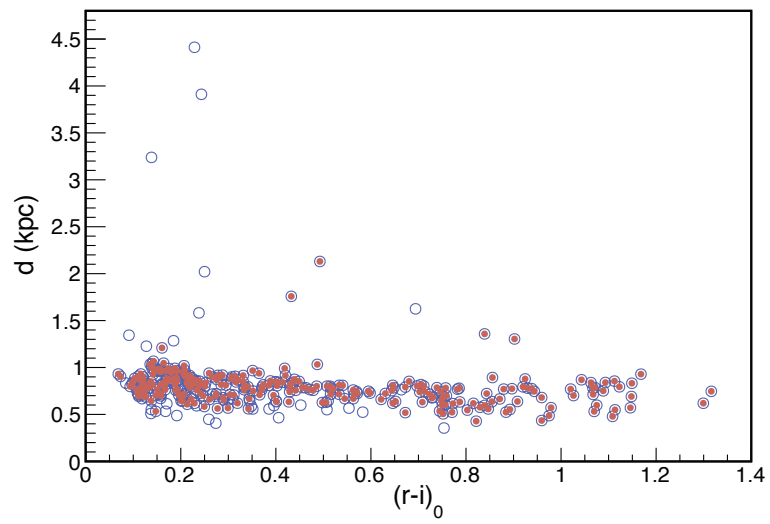


Fig. 6.— Same as Fig. 5 but using our $(r - i)_0$ based photometric parallax relation.

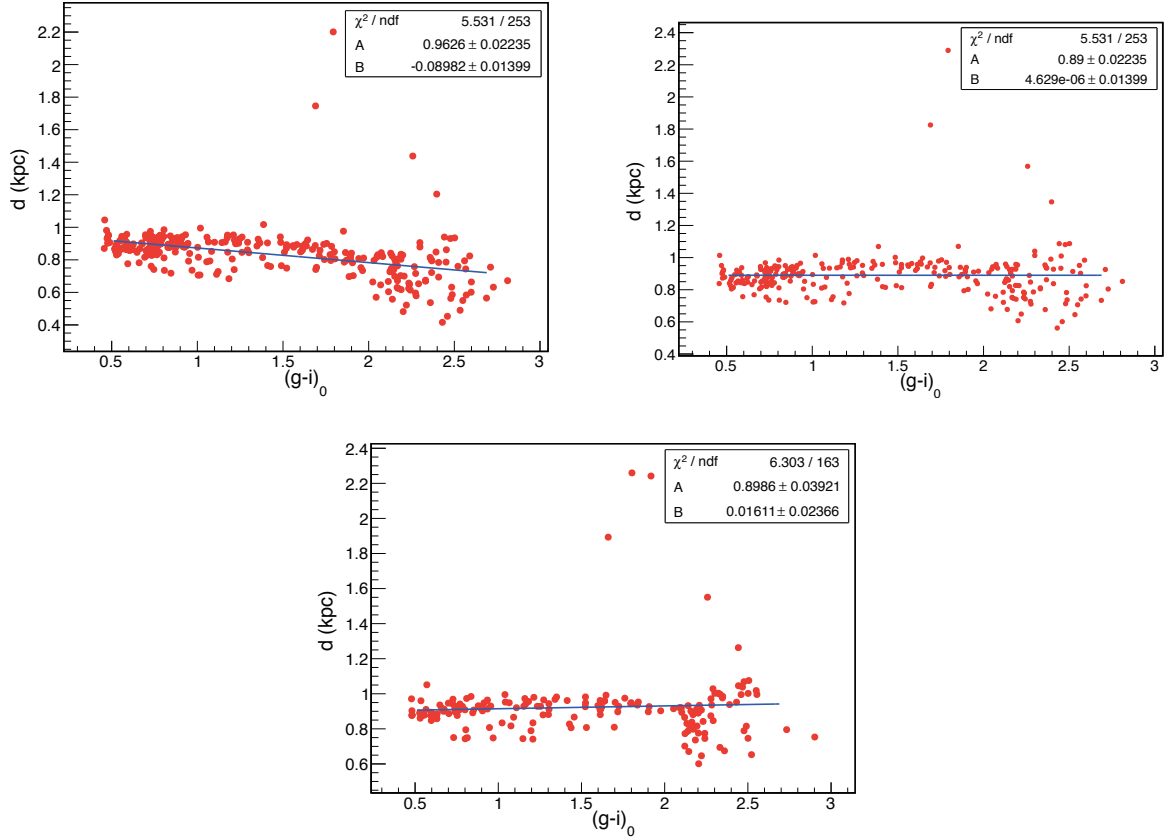


Fig. 7.— Our final steps in refining the $(g - i)_0$ photometric parallax relation and assessing systematic and statistical errors: the upper left panel shows the fit to the cleaned DR7 M67 sample of Fig. 5. After removing a linear slope to establish our adopted photometric parallax relation, the updated distances are fit and shown in the panel at the upper right. The small inset box lists the fit parameters (see text). The lower panel shows the updated photometric parallax relation determined from the DR7 fit applied to the DR9 sample, after a similar cleaning procedure has been applied.

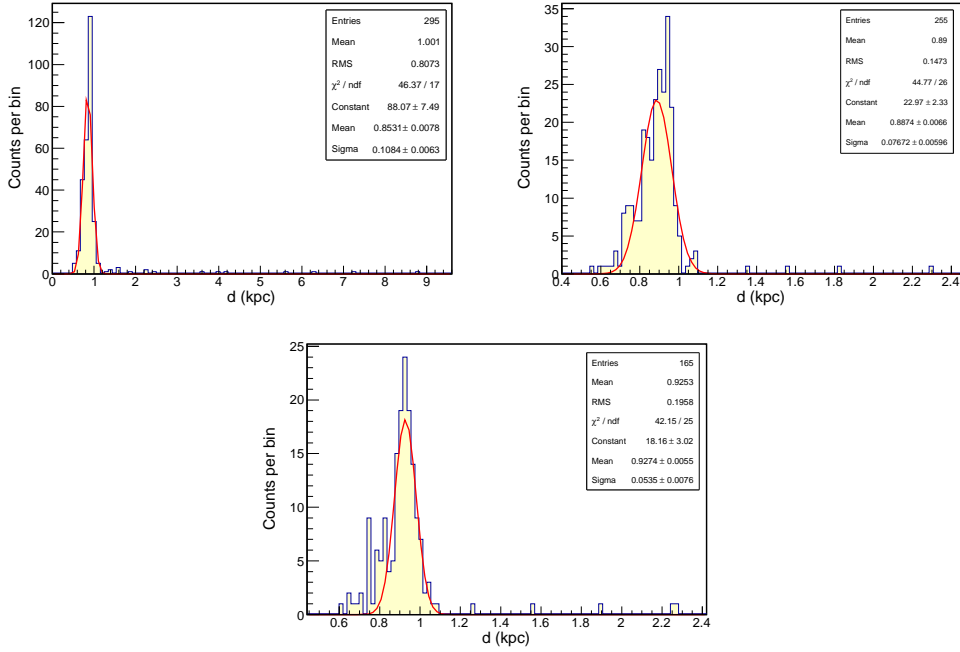


Fig. 8.— Gaussian fits to histograms of distance, starting with the complete (uncleaned) data set of Fig. 5 and using our refinement of Eq. (2) for the stellar distances. The RMS of the histogram is significantly larger than the standard deviation σ of the Gaussian fit (see “sigma” of the inset box), consistent with the long tail of non-Gaussian outliers which appear. The upper right panel contains a histogram of and a fit to only the cleaned data set, and now the histogram RMS and σ agree within a factor of two. The lower panel shows the fit to the cleaned DR9 sample. From these histograms we can estimate accurate statistical and systematic errors in the photometric parallax distance to M67.

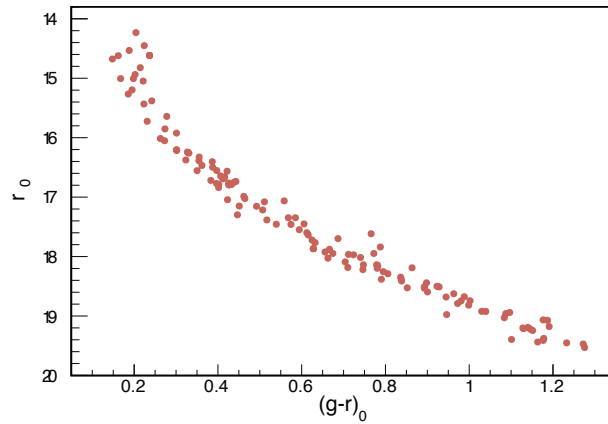


Fig. 9.— Color magnitude diagram of stars in the NGC 2420 field with radial velocity close to that of the known cluster value. Nearly all outliers are removed by this procedure.

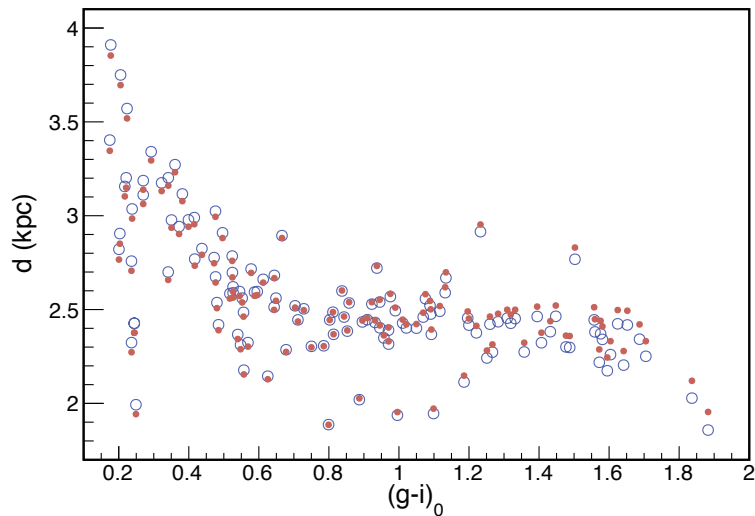


Fig. 10.— Photometric parallax relation of Fig. 7 applied to NGC 2420 candidate members, after applying the radial velocity cut (see text). Open circles are the distances after applying Eq. (2). The filled points represent the NGC 2420 stars after the same correction that was derived for M67, to yield the upper right panel of Fig. 7, is applied here. Note that we use $[\text{Fe}/\text{H}] = -0.37$ for the metallicity of the NGC 2420 stars.

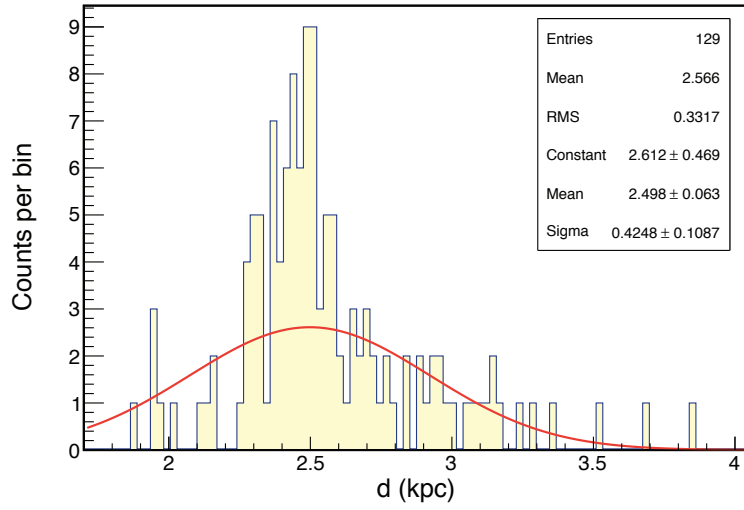


Fig. 11.— A photometric parallax histogram and fit to the DR9 NGC2420 candidate data set. The histogram RMS and Gaussian sigma are comparable, though both are broader than for the M67 data, suggesting the presence of non-cluster members.

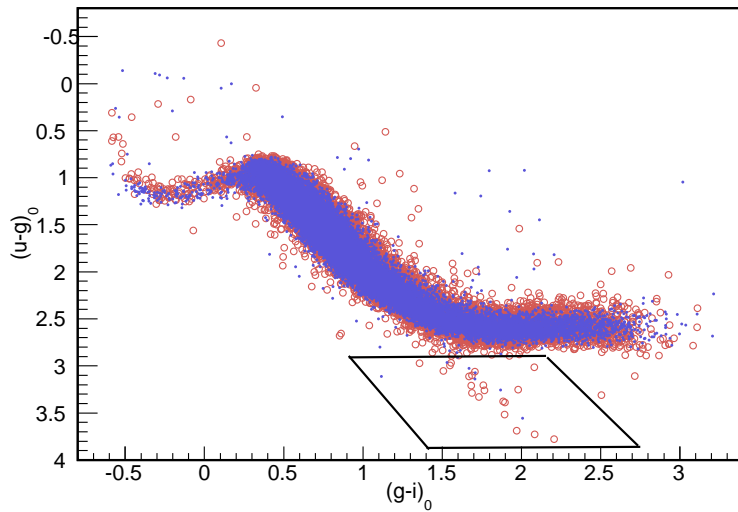


Fig. 12.— Color-color diagram of $(u-g)_0$ versus $(g-i)_0$ to identify non-main-sequence stars. We compare the population north and south: $b > 0$ (northern) stars are small, filled circles, whereas $b < 0$ (southern) stars are open circles. Here we only include objects with a u -band error of less than 0.05 and with $14.9 < r_0 < 15.4$. This selection favors brighter stars and thus giants over dwarfs. A fainter selection in r_0 would reduce the fraction of giants even further. Nearly all the stars in this plot are dwarfs; however, giants do appear and can be seen as a faint tail (mostly Sagittarius stream K/M giants) extending out of the dense stellar locus with $(g-i)_0 > 1.4$ and $(u-g)_0 > 3$. Giants are a completely negligible contaminant to our asymmetry analysis, for which $15 < r_0 < 21$ (see text).

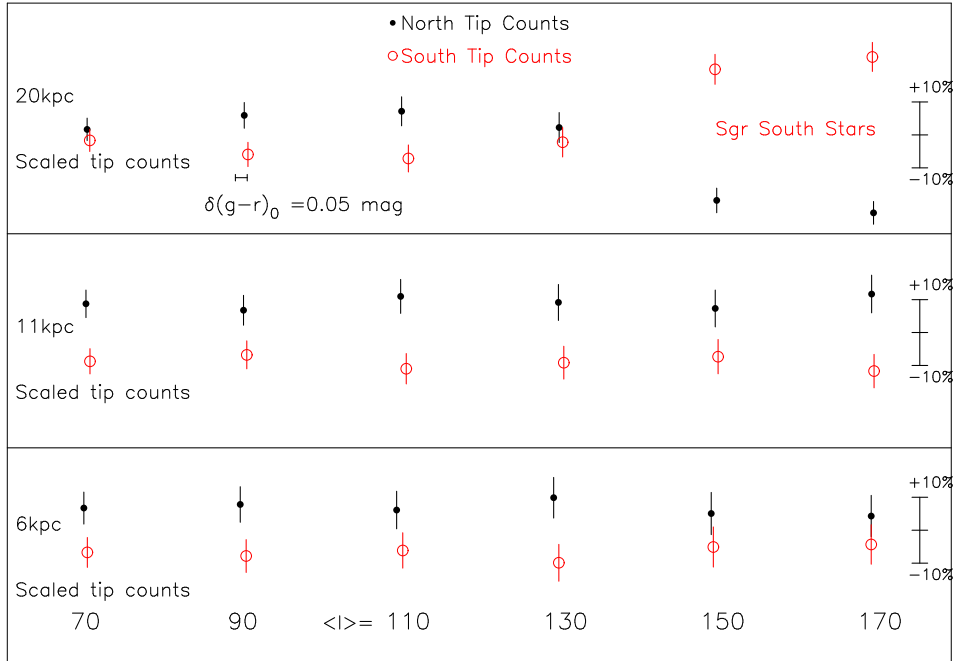


Fig. 13.— A graphical representation of Table 1, the fraction of blue-tip stars in the North and South with g_0 -band and l selection. The top row represents the most distant stars, having $20 < g_0 < 21$ ($d \sim 20$ kpc), and the error bars on each point are \sqrt{N} number-count statistics, and the points themselves are normalized by the sum of counts, North and South for that g_0 - and l -band selection (see the scale bar to the right for the fractional differences in counts). The middle panel is for stars with $19 < g_0 < 20$, and the lowest are for stars with $18 < g_0 < 19$, which are the nearest stars. Note in particular the horizontal shift between North-South pairings as one moves from left to right. This shift is the average shift in the peak of the blue-tip in $(g-r)_0$ color, the small horizontal scale bar in the top panel indicates a 5% shift.

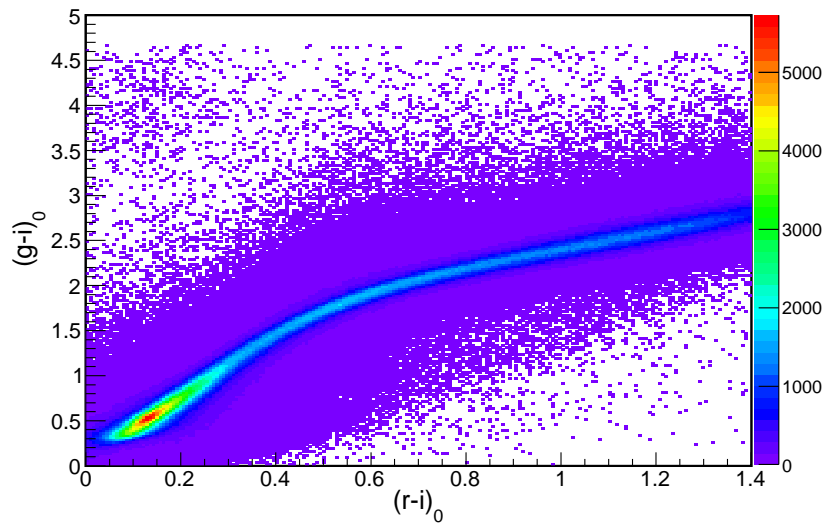


Fig. 14.— A $(r - i)_0$ versus $(g - i)_0$ color-color diagram for our stars — the smooth, tight correlation between the colors not only implies that the two different photometric parallax relations should be well-behaved but also suggests that they should give similar distance errors.

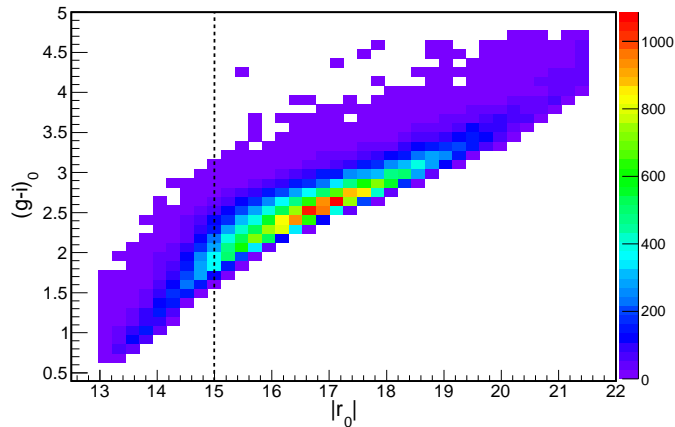


Fig. 15.— A $(g - i)_0$ versus r_0 CMD for stars with $|z| < 0.3$ kpc, computed as per Eq. (3). Here we explore the appropriate bright-end limit of our data set, noting that saturation begins to impact some colors strongly for stars with $r_0 \sim 14.5$ and brighter. We set the saturation cut at $r_0 = 15$ (vertical line) and exclude all brighter stars, in order to make the bright-end limit more uniform in color.

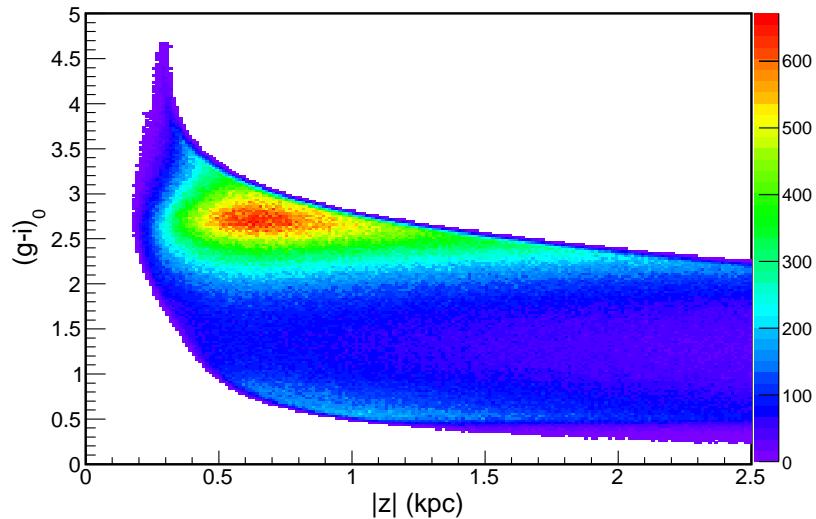


Fig. 16.— A color-distance diagram for our K/M dwarf sample. This figure of $(g - i)_0$ versus the absolute distance above the plane $|z|$ allows us to determine the range in $|z|$ over which a given band of $(g - i)_0$ color is complete (see text for the precise cuts used).

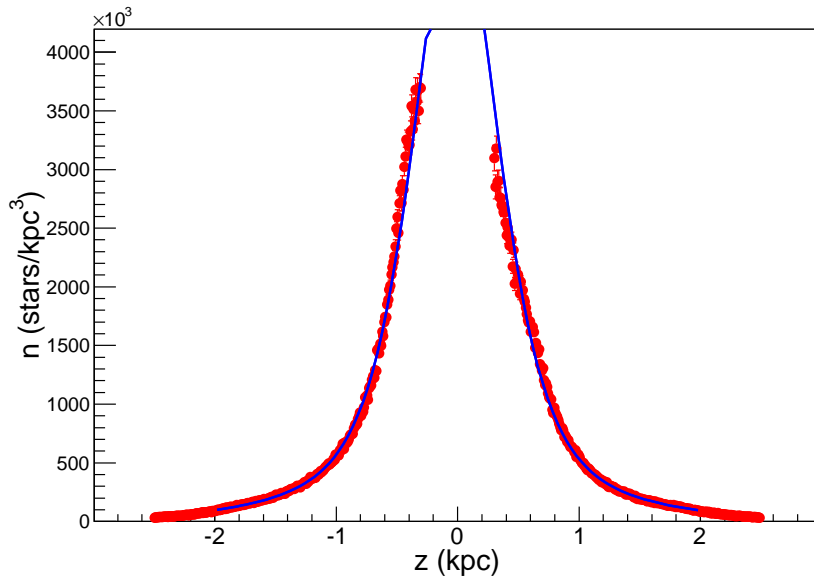


Fig. 17.— Histogram of the stellar density as a function of the vertical displacement z from the sun. We employ the selection function and color and saturation cuts described in the text and compute distances using Eq. (3). Even at this coarse scale, the wave-like North-South asymmetry can be seen on top of the symmetrical model.

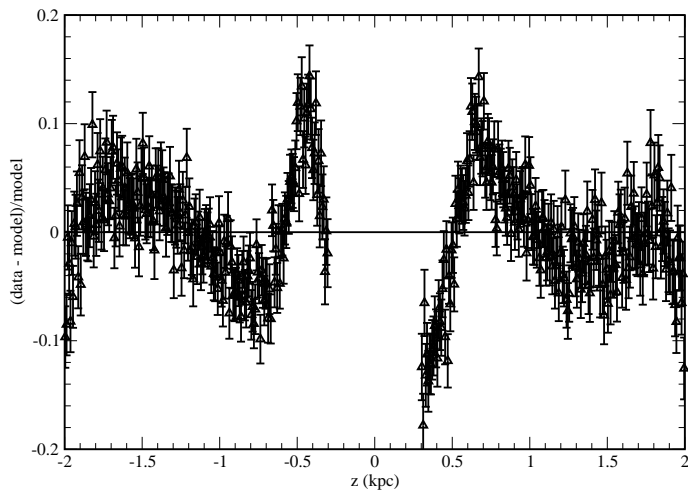


Fig. 18.— Difference between the estimated true stellar density and the best-fit model with vertical displacement from the sun, plotted as $(\text{data} - \text{model})/\text{model}$, determined from the inputs to Fig. 17. The residuals are dominantly of odd parity under $z \rightarrow -z$.

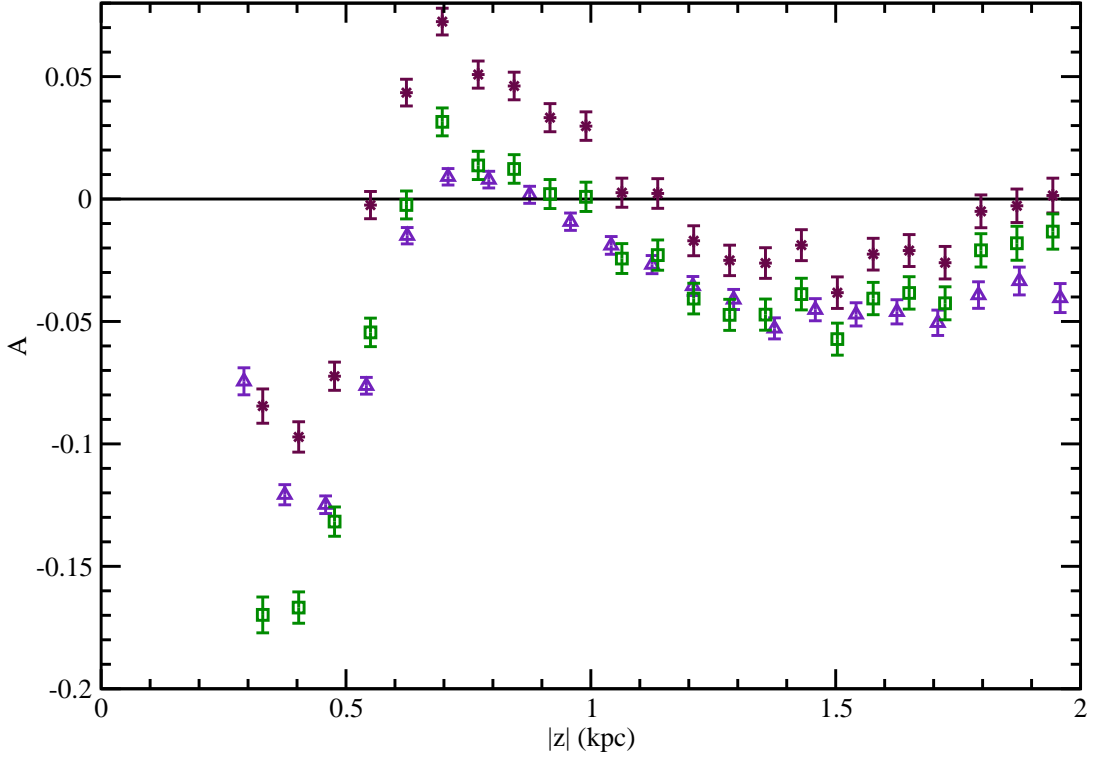


Fig. 19.— The asymmetry in star counts, North and South, with height $|z|$, using $(g - i)_0$ parallax with $1.8 < (g - i)_0 < 2.4$, through stages of the analysis. The triangular (purple) points show the asymmetry in observed star counts, $\mathcal{A}_{\text{raw}}(z)$ (see text), where $z = 0$ in this case is referenced to the sun’s location. The square (green) points show the asymmetry in observed star counts with z replaced by $z + z_\odot$ so that the origin is now the center of the Galactic plane, though the points are plotted on the same scale. We have used $z_\odot = 14.3$ pc. The asterisk (maroon) points show our final North-South asymmetry $\mathcal{A}(z + z_\odot)$ (see text); here, too, the origin is the center of the Galactic plane. In this case the selection function has been applied as well.

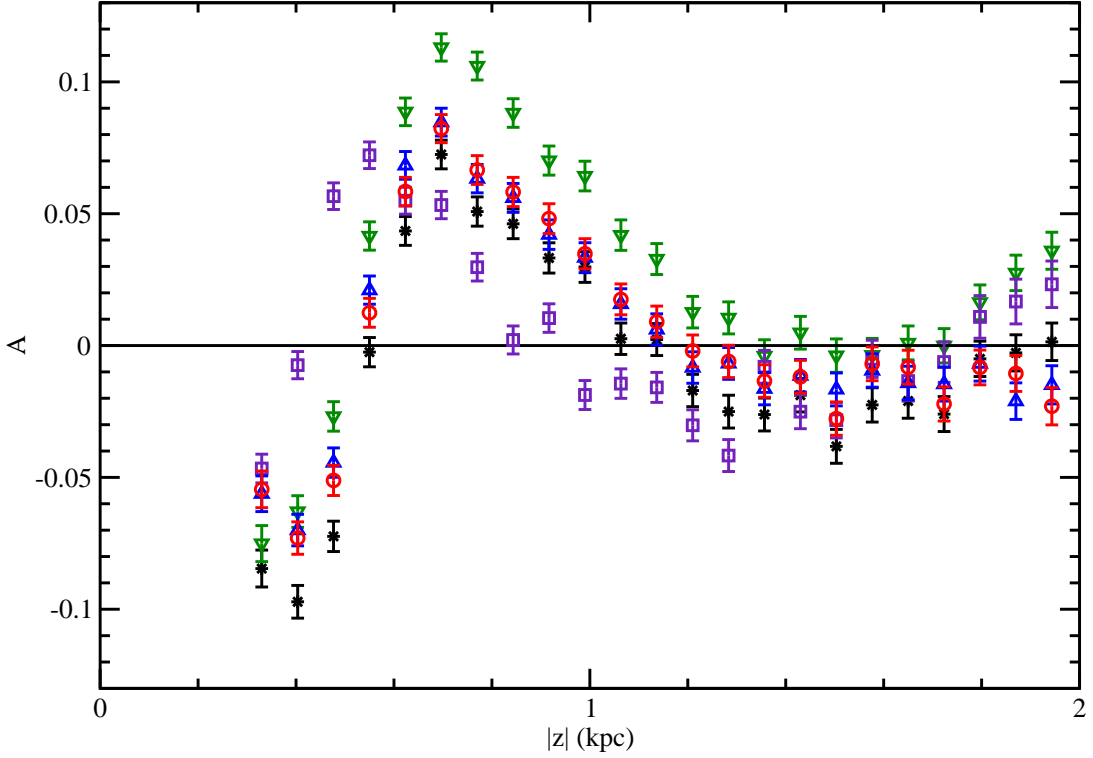


Fig. 20.— The asymmetry in star counts, North and South, with height $|z|$ from the center of the Galactic plane, using $(g - i)_0$ parallax with $1.8 < (g - i)_0 < 2.4$, upon the variation of different systematic effects. The asterisk (black) points show our final North-South asymmetry of Fig. 19, for which we use $z_\odot = 14.3$ pc, determined from the fit of our star counts. The down-pointing triangular (green) points show the asymmetry which emerges if z_\odot is changed to 30 pc. The square (purple) points shows the asymmetry if the adjustment of the photometric parallax relation from the fit of the M67 cluster, Eq. (3), is not employed. The last two curves illustrate the consequence of a possible 2% g -band calibration error on the asymmetry. The up-pointing triangular (blue) points shows the asymmetry which emerges if $g \rightarrow g + 0.02$ in the North only, and the circular (red) points illustrate what happens if $g \rightarrow g - 0.02$ in the South only.

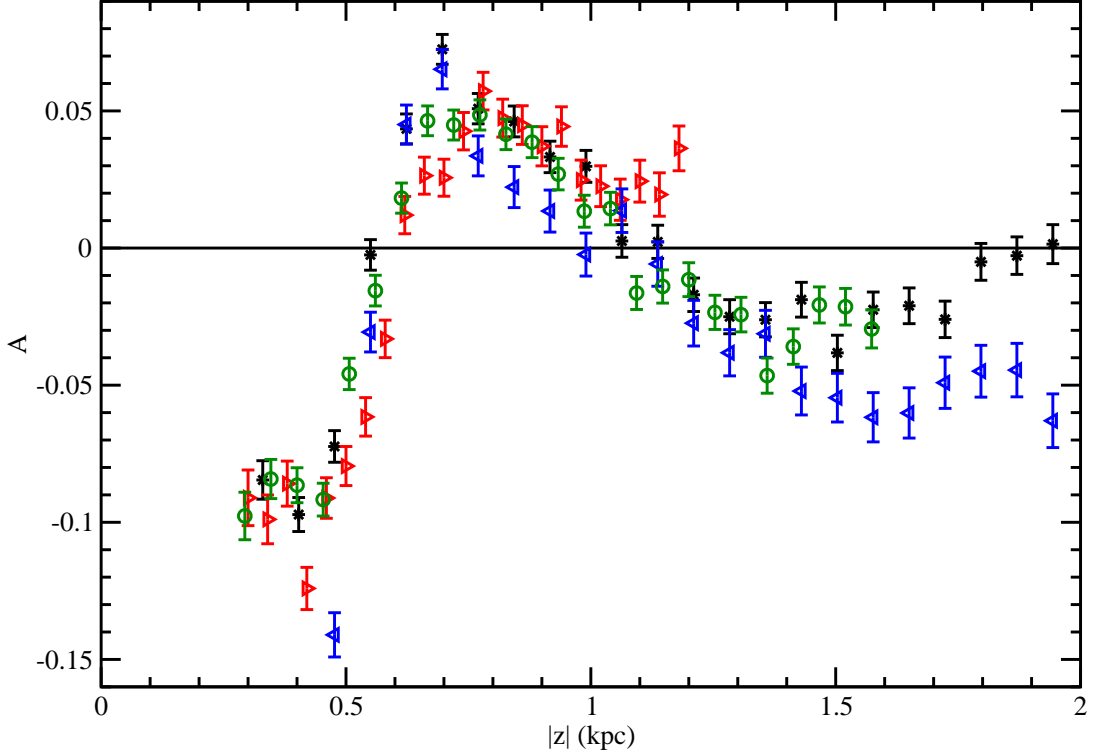


Fig. 21.— The asymmetry in star counts, North and South, with height $|z|$ from the Galactic plane, for different bands in $(g - i)_0$ color. The asterisk (black) points correspond to $1.8 < (g - i)_0 < 2.4$; these points are the same as the asterisk points depicted in Fig. 19. The left-pointing-triangle (blue) correspond to $0.95 < (g - i)_0 < 1.8$, whereas the right-pointing-triangle (red) points correspond to $2.4 < (g - i)_0 < 2.7$. We also include an asymmetry analyzed using our distance relationship based on $(r - i)_0$ color, Eq. (4); the circle (green) points correspond to $0.6 < (r - i)_0 < 1.1$. In each case the window in $|z|$ shown is determined by the r_0 saturation limits for the given color interval, as determined, e.g., for $(g - i)_0$ color from Fig. 16. We employ $z_\odot = 14.3$ pc throughout, and emphasize that $|z| = 0$ here is referenced to the center of the Galactic plane.

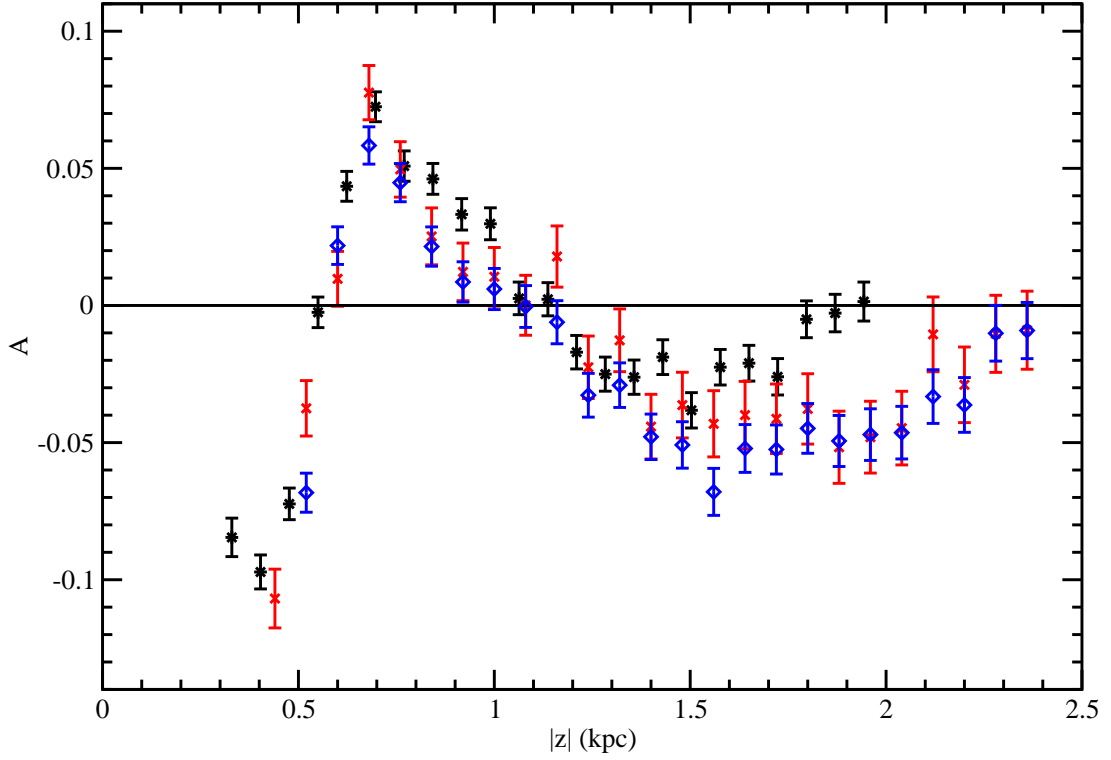


Fig. 22.— The asymmetry in star counts, North and South, with height $|z|$ from the Galactic plane, for different bands in $(g - i)_0$ color. The asterisk (black) points correspond to $1.8 < (g - i)_0 < 2.4$; these points are the same as the asterisk points depicted in Figs. 19 and 21. The diamonds (blue) correspond to $0.95 < (g - i)_0 < 1.8$, whereas the crosses (red) correspond to $1.4 < (g - i)_0 < 1.8$ — some of the “contamination” in the $|z| \sim 1.5$ kpc region is removed through this more restricted color cut, but the data seem to suggest the existence of a nonzero asymmetry at these heights as well.

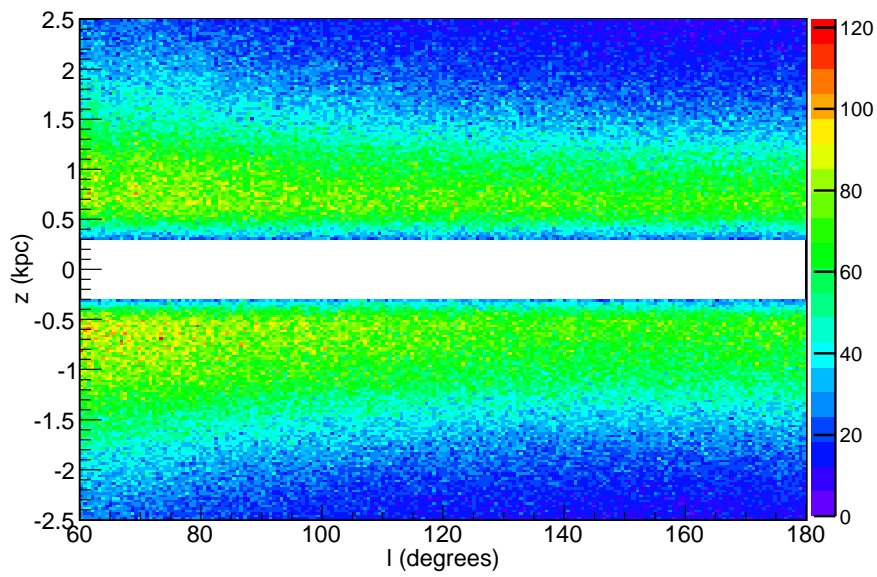


Fig. 23.— The stellar number counts with height $|z|$ from the Galactic plane, using $(g - i)_0$ parallax with $0.95 < (g - i)_0 < 2.7$, and with l . We have imposed that $|r_0| > 15$ and that $0.3 < |z| < 2.5$ kpc. This is the sample employed in our analysis of the asymmetry in North-South number counts with l .

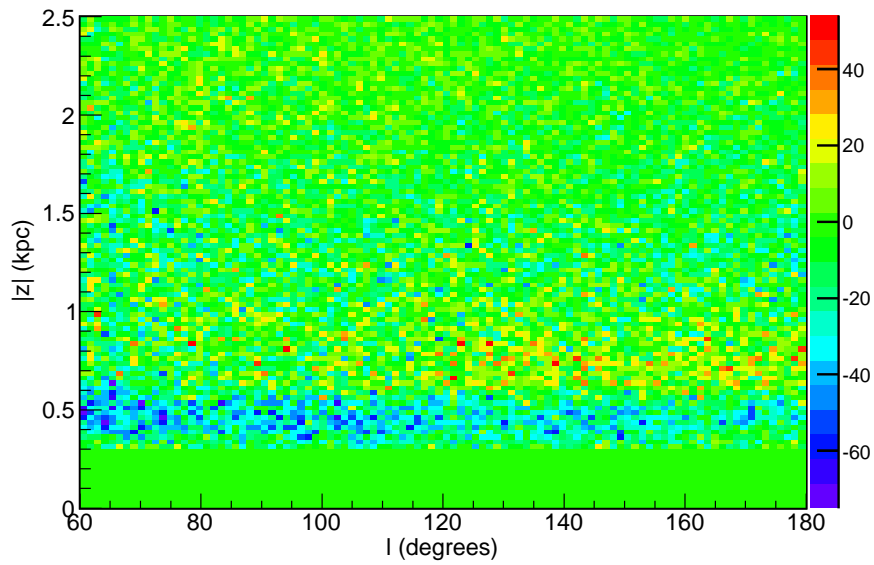


Fig. 24.— The difference in the stellar number counts, North minus South, with height $|z|$ from the Galactic plane, using $(g - i)_0$ parallax with $0.95 < (g - i)_0 < 2.7$, and with l . This is realized from the data displayed in Fig. 23 and thus contains the same cuts. The features of the asymmetry presented in Fig. 25 are already apparent in the raw data, as we show here.

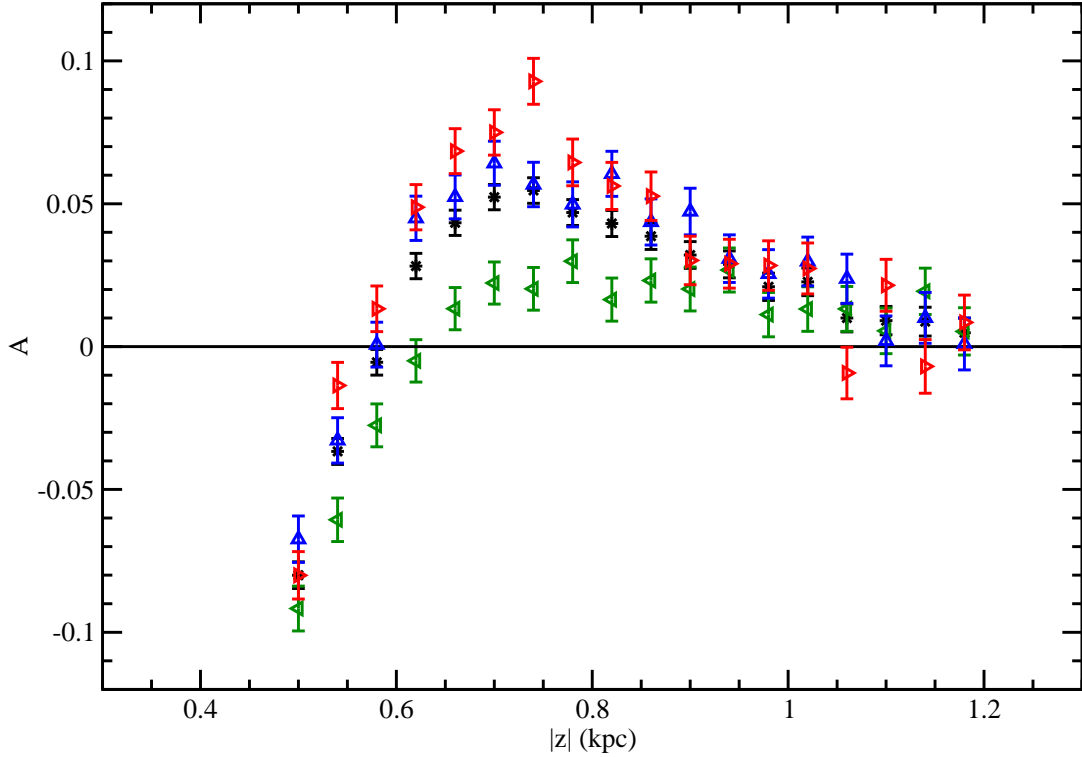


Fig. 25.— The asymmetry in star counts, North and South, with height $|z|$ from the Galactic plane, using $(g-i)_0$ parallax with $0.95 < (g-i)_0 < 2.7$, for different ranges in l . The asterisk (black) points are the results for our complete range in l , $60^\circ \leq l \leq 180^\circ$. The left-pointing triangles (green) correspond to $60^\circ \leq l \leq 100^\circ$. The up-pointing triangles (blue) correspond to $100^\circ \leq l \leq 140^\circ$, and the right-pointing triangles (red) have $140^\circ \leq l \leq 180^\circ$. As in Fig. 21 we employ $z_\odot = 14.3$ pc throughout, while $|z| = 0$ is referenced to the center of the Galactic plane.